



# Candida pathogens induce protective mitochondria-associated type I interferon signalling and a damage-driven response in vaginal epithelial cells

Marina Pekmezovic<sup>1,12</sup>, Hrant Hovhannisan<sup>1,2,3,10,11,12</sup>, Mark S. Gresnigt<sup>1,4</sup>, Elise Iracane<sup>1,5</sup>, João Oliveira-Pacheco<sup>5</sup>, Sofía Siscar-Lewin<sup>1</sup>, Eric Seemann<sup>1,6</sup>, Britta Qualmann<sup>6</sup>, Till Kalkreuter<sup>1</sup>, Sylvia Müller<sup>7</sup>, Thomas Kamradt<sup>7</sup>, Selene Mogavero<sup>1</sup>, Sascha Brunke<sup>1</sup>, Geraldine Butler<sup>1,5</sup>, Toni Gabaldón<sup>1,2,3,8,10,11,13</sup>✉ and Bernhard Hube<sup>1,9,13</sup>✉

Vaginal candidiasis is an extremely common disease predominantly caused by four phylogenetically diverse species: *Candida albicans*; *Candida glabrata*; *Candida parapsilosis*; and *Candida tropicalis*. Using a time course infection model of vaginal epithelial cells and dual RNA sequencing, we show that these species exhibit distinct pathogenicity patterns, which are defined by highly species-specific transcriptional profiles during infection of vaginal epithelial cells. In contrast, host cells exhibit a homogeneous response to all species at the early stages of infection, which is characterized by sublethal mitochondrial signalling inducing a protective type I interferon response. At the later stages, the transcriptional response of the host diverges in a species-dependent manner. This divergence is primarily driven by the extent of epithelial damage elicited by species-specific mechanisms, such as secretion of the toxin candidalysin by *C. albicans*. Our results uncover a dynamic, biphasic response of vaginal epithelial cells to *Candida* species, which is characterized by protective mitochondria-associated type I interferon signalling and a species-specific damage-driven response.

Vulvovaginal candidiasis (VVC) is among the most common fungal infections, affecting 70–75% of women at least once in their lifetime<sup>1</sup>. VVC is characterized by acute inflammation of the vaginal mucosa due to the overgrowth of normally commensal *Candida* species<sup>2–4</sup>. Although *Candida albicans* is the predominant cause of VVC, the prevalence of species like *Candida glabrata*, *Candida parapsilosis* and *Candida tropicalis* has increased (reviewed in Makanjuola et al.<sup>5</sup>). Despite the shared genus name, these species are phylogenetically diverse and often have non-pathogenic close relatives, indicating that their ability to infect humans has emerged independently<sup>6</sup>. How these diverse *Candida* species interact with host cells has rarely been addressed on a comparative basis. Improved knowledge of similarities and species-specific characteristics of infection processes is crucial to understand the pathogenesis, improve diagnostics and therapy of candidiasis<sup>7</sup>.

Research on host-fungi interactions has mainly focused on immune cells, which are considered crucial players in the defence against fungal infections<sup>8,9</sup>. However, epithelial cells play a fundamental role in shaping the host defence against fungi, which goes beyond their function as a physical barrier<sup>10–15</sup>.

Studies in infection biology often focus on either the pathogen or host response, yet microbial pathogenesis can be best interpreted in the framework of dynamic host-microbe interactions. Dual RNA sequencing (RNA-seq) enables the combined assessment of the transcriptional responses of host and pathogen<sup>16,17</sup> and provides insights into the interactions of fungal pathogens with different host cells<sup>17–23</sup>.

To elucidate general and species-specific interactions between vaginal epithelial cells and the four most prevalent VVC-causing *Candida* species, we applied dual RNA-seq and an in vitro infection model. Our experimental design allows pathogens to deploy their arsenal of pathogenicity factors without restriction by the immune system. Furthermore, it facilitates specific investigation of epithelial recognition and defence mechanisms, which constitute the first line of defence against infecting fungi.

Our results reveal that fungal transcriptomes show species-specific patterns during infection, probably reflecting the independently evolved pathogenic potential of *Candida* species. Vaginal epithelial cells display a biphasic response: an early protective type I interferon (IFN) response, which is mediated by sublethal

<sup>1</sup>Department of Microbial Pathogenicity Mechanisms, Leibniz Institute for Natural Product Research and Infection Biology, Hans Knoell Institute, Jena, Germany. <sup>2</sup>Bioinformatics and Genomics Programme, Centre for Genomic Regulation, Barcelona Institute of Science and Technology, Barcelona, Spain.

<sup>3</sup>Universitat Pompeu Fabra, Barcelona, Spain. <sup>4</sup>Junior Research Group Adaptive Pathogenicity Strategies, Leibniz Institute for Natural Product Research and Infection Biology, Hans Knoell Institute, Jena, Germany. <sup>5</sup>School of Biomedical and Biomolecular Science and UCD Conway Institute of Biomolecular and Biomedical Research, Conway Institute, University College Dublin, Dublin, Ireland. <sup>6</sup>Institute for Biochemistry I, Jena University Hospital-Friedrich Schiller University, Jena, Germany. <sup>7</sup>Institute of Immunology, Universitätsklinikum Jena, Jena, Germany. <sup>8</sup>Institució Catalana de Recerca i Estudis Avançats, Barcelona, Spain. <sup>9</sup>Institute of Microbiology, Friedrich Schiller University, Jena, Germany. <sup>10</sup>Present address: Life Sciences Department, Barcelona Supercomputing Center, Barcelona, Spain. <sup>11</sup>Present address: Mechanisms of Disease Department, Institute for Research in Biomedicine, Barcelona, Spain.

<sup>12</sup>These authors contributed equally: Marina Pekmezovic, Hrant Hovhannisan. <sup>13</sup>These authors jointly supervised this work: Toni Gabaldón, Bernhard Hube. ✉e-mail: [toni.gabaldon.bcn@gmail.com](mailto:toni.gabaldon.bcn@gmail.com); [bernhard.hube@leibniz-hki.de](mailto:bernhard.hube@leibniz-hki.de)

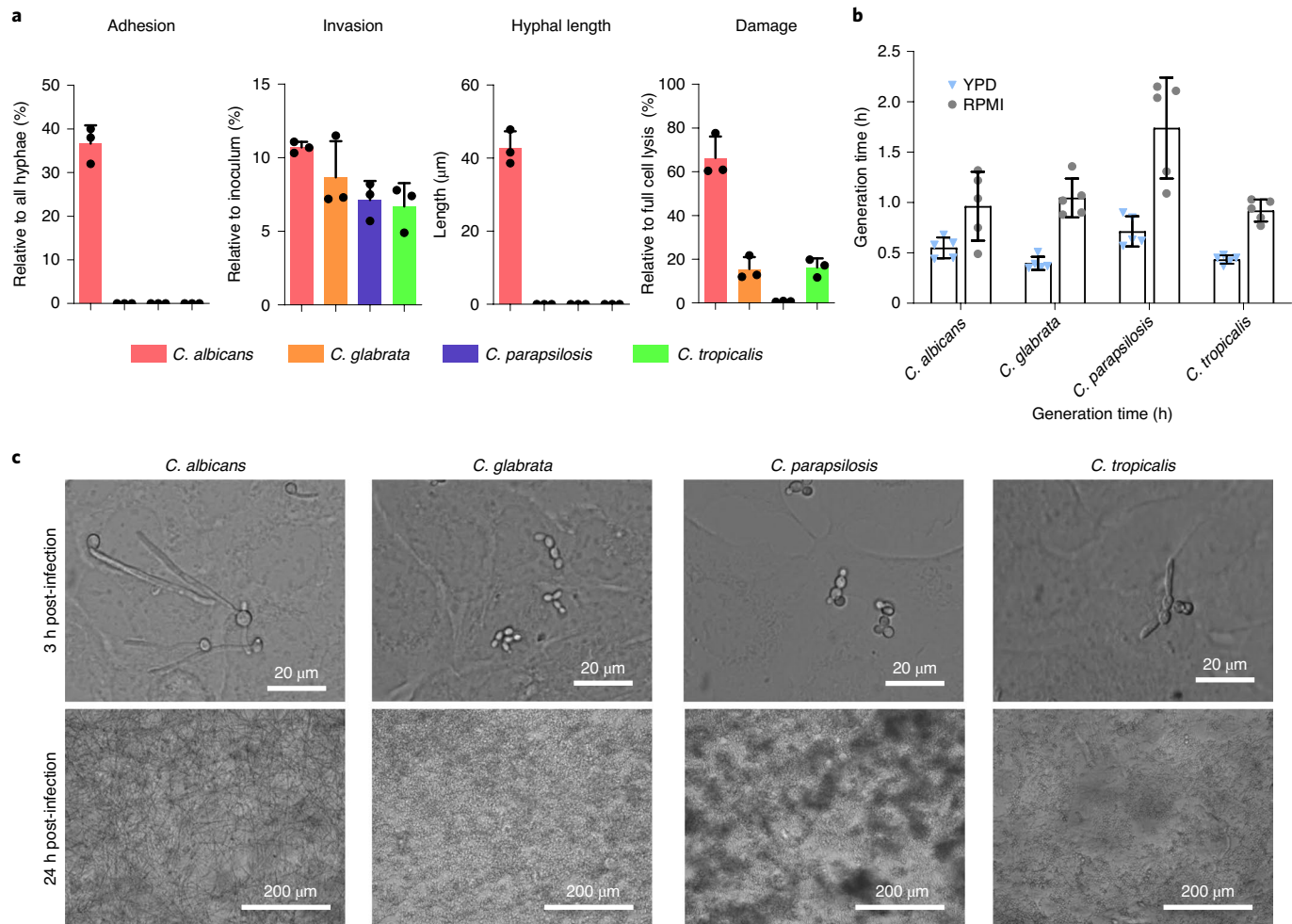


**Fig. 1 | Pathogenicity patterns of four *Candida* species in the in vitro vaginal epithelial infection model.** **a**, Adhesion, determined as the percentage of *Candida* cells from the original inoculum that adhered to vaginal epithelial cells at 1 h post-infection; invasion, determined as the percentage of *Candida* cells that invaded the vaginal epithelial cells at 3 h post-infection; hyphal length (μm) recorded at 3 h post-infection; necrotic damage, measured by the quantification of LDH activity in the supernatant and presented as a percentage relative to total lysis (maximum damage control) at 24 h post-infection. All values are presented as mean  $\pm$  s.d. of  $n=3$  independent in vitro infection experiments. **b**, Generation times of *Candida* species in YPD or RPMI 1640 medium (used for vaginal epithelial cell infections) measured in 24-h growth curves. All values are presented as the mean  $\pm$  s.d. of  $n=5$  independent experiments. No statistically significant difference in growth between species in either YPD nor RPMI was observed (one-way ANOVA with Greenhouse-Geisser correction and Tukey's multiple comparisons test). **c**, Micrographs of *Candida* morphology at 3 h post-infection and confluent biofilms at 24 h post-infection on vaginal epithelial cells. Micrographs are representative of  $n=3$  independent experiments with similar results.

mitochondrial signalling; and a damage-associated late response that depends on species-specific pathogenicity mechanisms.

## Results

**Candida species-specific pathogenicity patterns.** To study the interaction of the four most common *Candida* species causing VVC with vaginal epithelial cells, we first assessed their adhesion, invasion and damage potential as well as their growth rates and morphologies (Fig. 1a). Despite the similar adhesion rates of all species, only *C. albicans* switched to hyphal growth, invaded epithelial cells and induced necrotic cell damage. Non-invading *C. glabrata* and *C. tropicalis* caused low damage levels. *C. glabrata* grew only in the yeast morphology, whereas occasional pseudohyphae were observed for *C. tropicalis*. Finally, *C. parapsilosis* remained in the yeast morphology during the entire course of infection, forming cell aggregates, but did not invade or cause damage. All species exhibited similar growth rates (Fig. 1b) and showed a biofilm layer 24 h post-infection, thus excluding the possibility that differences in epithelial damage resulted from different proliferation rates (Fig.

1c). These results show species-specific pathogenicity patterns, involving different morphologies, levels of invasion and damaging capacity.

**Species-specific transcriptional responses to epithelial cells.** Subsequently, we investigated whether these differential pathogenicity patterns were reflected in the transcriptional responses of both fungal and epithelial cells (see the experimental set-up in Extended Data Fig. 1 and cross-mapping analysis between human and yeast sequencing reads in Supplementary Files 1–4). The transcriptional dynamics of each *Candida* species throughout the infection were analysed (Fig. 2). All species induced rapid transcriptional responses following infection with increasing numbers of differentially expressed genes over the course of infection (Fig. 2a and Supplementary Files 5–8). Gene Ontology (GO) enrichment analysis revealed the function of differentially expressed genes (Fig. 2b and Supplementary File 9). We observed species-specific functional enrichments, albeit with some commonalities. At 3 h post-infection, *C. albicans* and *C. glabrata* activated carbohydrate catabolic

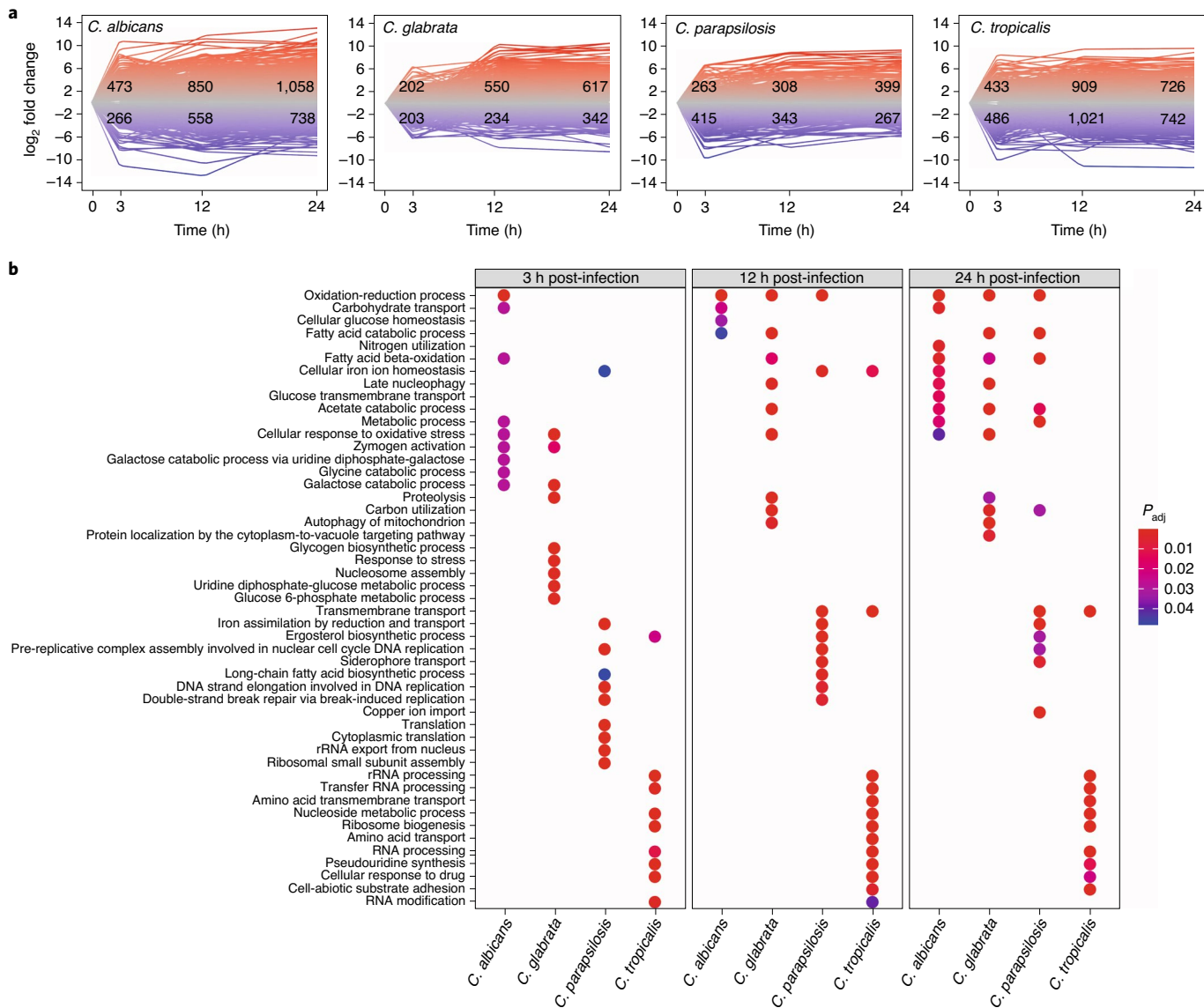


**Fig. 2 | Dynamics of transcriptomic changes of the four *Candida* species investigated in this study at different time points.** **a**, *Candida* species transcriptome dynamics plots from RNA-seq data based on  $\log_2$ (fold change) of expression during the course of infection compared to *Candida* adapted to RPMI culture medium (time point 0). Each line corresponds to the relative fold change of expression levels of a single gene. The numbers on the plots indicate a number of differentially expressed genes ( $\log_2$ (fold change) > 1.5,  $P_{adj} < 0.01$ , upregulated (red), downregulated (blue)). **b**, GO term enrichment analysis of upregulated genes (category ‘biological process’) in the four *Candida* species. The x axis indicates the fungal species, the y axis indicates GO terms. Only significant ( $P_{adj} < 0.05$ ) GO enrichments are shown. Differentially expressed gene analyses were done using DESeq2 v.1.26.0; comparisons against time point 0 were done using the two-sided Wald test. GO enrichment analysis was done using clusterProfiler v.3.14.3, which was used to perform the hypergeometric test. Adjustments of P values for differentially expressed gene and GO enrichment were done by Benjamini-Hochberg procedure. See Supplementary File 9 for the full list of enriched GO terms for each species, time point, up- or downregulation and GO category.

processes and stress response pathways. *C. parapsilosis* upregulated, among others, genes related to iron transport, ribosome assembly and translation. In contrast, *C. tropicalis* differentially expressed genes were mainly related to RNA processing, ribosome biogenesis and ergosterol biosynthetic processes. At later stages, similar functional enrichments were observed across the species. The GO terms oxidation-reduction process, fatty acid beta-oxidation, iron homeostasis and acetate catabolism were enriched in at least three species throughout the infection.

When comparing differentially expressed genes across species, a remarkably distinct pattern was observed for each pathogen

(Extended Data Fig. 2). Analysis of the distribution of species-specific (without orthologues in the other species), partially shared (with orthologues in one or two of the other species) and fully shared (1-to-1 orthologous genes in all species) differentially expressed genes (Extended Data Fig. 2a) revealed that species-specific and partially shared genes constitute a substantial proportion (31–72%). Moreover, species-specific genes are more likely to be differentially expressed than fully shared genes (chi-squared test  $P < 0.05$ , except for *C. tropicalis*). Even orthologous genes present in all four species showed species-specific differential expression (Extended Data Fig. 2b). Consistently, principal component analysis (PCA) based

on orthologous gene expression showed species-specific clusters (Extended Data Fig. 2c).

Gene coexpression analysis was used as an independent approach to investigate commonalities and differences of fungal transcriptional responses. By constructing host-pathogen interaction coexpression networks, highly interconnected gene clusters (modules) were defined and their biological functions were inferred by GO term analysis. In each fungal infection scenario, we detected numerous modules of coexpressed genes (22–28 modules; Supplementary File 10).

Based on fully shared genes, we then assessed whether the fungal genes in the coexpressed modules were conserved across species. Distinct modules were observed for each *Candida* species with few shared genes. On average, only 5% of orthologous genes were shared between any modules of different species (Extended Data Fig. 3). Therefore, the genes in the coexpression modules functionally showed a large species specificity (Supplementary File 10) with few exceptions. The modules with the highest similarity, that is, module3 in *C. glabrata* and module3 in *C. tropicalis*, were both enriched for genes associated with DNA replication. Interestingly, we observed modules related to adhesion in *C. albicans* (module11) and *C. tropicalis* (module13), respectively, possibly related to shared virulence features of these two species.

**Infection-specific differentially expressed genes of *Candida* species.** Comparisons of *C. albicans* gene expression during infection of oral epithelium or vascular endothelium, and growth in the tissue culture medium, revealed that only a fraction of genes were specifically expressed during interactions with host cells<sup>20</sup>. This indicates that most of the genes induced during interaction with the host are also required for growth in culture media.

To investigate whether such a phenomenon also occurs during interaction with vaginal cells, controls of fungal cells grown in culture medium only were investigated (Extended Data Fig. 1 and Supplementary Table 1). A subtraction of the differentially expressed genes in medium from those expressed on epithelial cells revealed a large overlap between the differentially expressed genes during infection and in culture medium (Fig. 4 and Supplementary Files 5–8). Infection-specific genes are mostly species-specific (Extended Data Fig. 4) and GO enrichment analysis identified different functional enrichments depending on the species (Supplementary File 9).

These were characterized by genes involved in mitochondrial electron transport and ATP synthesis for *C. glabrata*, ergosterol biosynthesis, sulphite and manganese ion transport for *C. parapsilosis* and ribosome biogenesis and ribosomal RNA processing for *C. tropicalis*. No functional enrichments were identified in the upregulated, infection-specific *C. albicans* genes, yet the downregulated genes showed enrichment in three GO terms related to white-opaque phenotypic switching. These downregulated genes include *WOR1*, a master regulator inducing the less virulent opaque state<sup>24</sup>.

In summary, distinct transcriptional patterns for each yeast species during infection were observed, suggesting highly species-specific strategies to cope with epithelial cells.

**Epithelial transcriptomic responses to *Candida* species.** To shed light on how the *Candida* species-specific pathogenicity and transcriptional patterns influence the host response, epithelial transcriptome responses to infections were analysed (Fig. 3a,b). The epithelial cell transcriptome dynamics showed a bias towards upregulation of genes at the initial stages of infection (Fig. 3a), which is consistent with previous findings<sup>25</sup>.

When compared against the total number of differentially expressed genes (Fig. 3c, top), the proportion of common differentially expressed genes induced by infection with any of the four species decreased throughout the time course—8.8% of common differentially expressed genes at 3 h post-infection, and 7.6 and 6.4% at 12 h and 24 h post-infection, respectively. A similar pattern is observed when comparing common differentially expressed genes to the differentially expressed genes induced specifically by each fungal species (Fig. 3c, bottom). The larger fraction of shared differentially expressed genes at the early time points suggests that the response to the different yeast species is more conserved at the early infection stages while increased species specificity is observed at the later stages (Fig. 3b,c).

PCA analysis of the gene expression of epithelial cells revealed a similar pattern (Fig. 3d). The tight clustering at 3 h post-infection indicates that epithelial cells exhibit a uniform transcriptional response to the four *Candida* species at the early stages of infection, in contrast to the fungal transcriptional profiles. However, the epithelial transcriptomes diverge from 12 h post-infection onwards; at 24 h post-infection we observed three distinct clusters of responses to the different species. The transcriptional response of epithelial cells to *C. tropicalis* and *C. glabrata* showed high similarity, being different from the responses to *C. albicans* or *C. parapsilosis*. Functional GO term enrichment analysis revealed a similar trend: at the early time point, GO terms associated with mitochondrial processes are enriched for all species and of type I interferon (IFN) responses for all species except *C. tropicalis*. At the later stages, species-specific terms appeared (Fig. 3e).

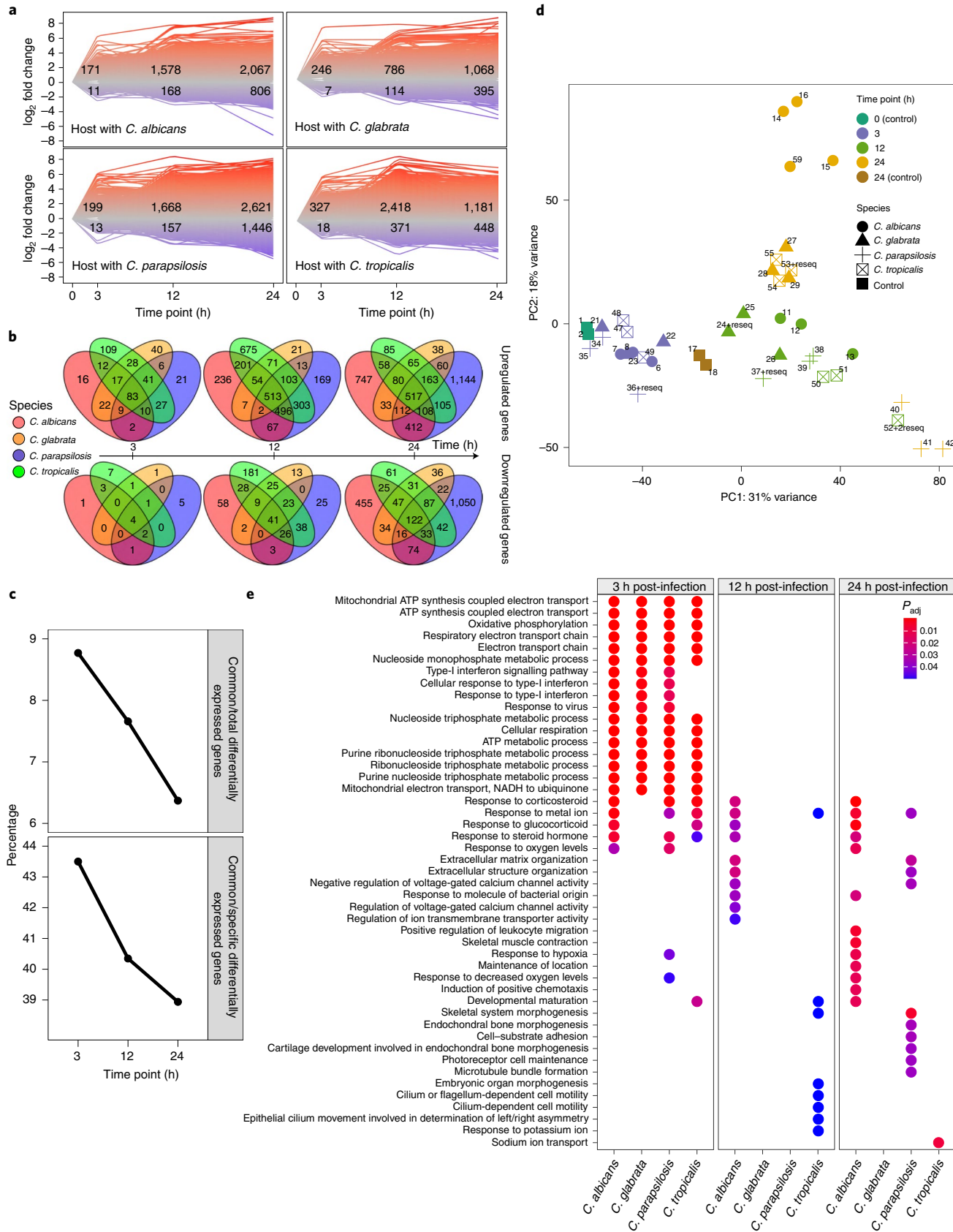
Based on these results, we decided to unravel the basis of the two observed key phenomena: (1) the uniform early transcriptional response related to mitochondria and type I IFN signalling; and (2) the divergence of the host transcriptome response at the later stages of infection.

**Uniform early responses to *Candida* infections.** The upregulation of genes associated with the respiratory electron transport chain (Fig. 3e) in epithelial cells at the early time points with all *Candida* species included induction of all mitochondrial genes (Fig. 4a). The response was dependent on viable fungi being in direct contact with the epithelial cells (RNA-seq, Extended Data Fig. 6 and Supplementary Files 5–8; quantitative PCR with reverse

**Fig. 3 | Transcriptome dynamics of vaginal epithelial cells on exposure to four *Candida* species.** **a**, Transcriptome dynamics plots from RNA-seq data based on  $\log_2(\text{fold change})$  compared to time point 0. Each line corresponds to the relative fold change of expression levels of a single gene. The numbers on the plots indicate the number of differentially expressed genes ( $\log_2(\text{fold change}) > 1.5$ ,  $P_{\text{adj}} < 0.01$ , upregulated (red), downregulated (blue)). **b**, Venn diagrams showing similarities and differences of human differentially expressed genes in response to *Candida* species. **c**, Proportion between shared differentially expressed genes and the total number of differentially expressed genes (top) and proportion between shared differentially expressed genes and the differentially expressed genes induced exclusively by each fungal species (bottom). **d**, PCA biplot of all analysed human samples. The labels of the data points correspond to sample identifiers, where 'reseq' indicates that the sample was sequenced more than once (Supplementary Table 1 for further details). **e**, GO term enrichment analysis for upregulated genes (category 'biological process') of the host at different time points. The x axis indicates the infecting *Candida* species. Only significant ( $P_{\text{adj}} < 0.05$ ) GO enrichments are shown. Differentially expressed gene analyses were done using DESeq2 v.1.26.0; comparisons against time point 0 were done using a two-sided Wald test. GO enrichment analysis was done using clusterProfiler v.3.14.3, which was used to perform the hypergeometric test. Adjustments of  $P$  values for differentially expressed gene and GO enrichment were done by Benjamini-Hochberg procedure.

transcription (RT-qPCR), Fig. 4a). Similarly, our coexpression network analysis identified host modules with functional enrichment of mitochondrial genes and oxidative phosphorylation across all

infections (Supplementary File 10). These observations suggest that mitochondria-associated processes are triggered in epithelial cells on infection with *Candida* species.



Host mitochondria have recently been identified as hubs of the innate immune responses<sup>26,27</sup>. In particular, mitochondrial signalling is known to activate type I IFN signalling pathways<sup>28</sup>. We observed enrichment of GO terms (Fig. 3e) and upregulation of interferon-stimulated genes (ISGs) associated with the type I IFN response<sup>29</sup> on exposure of epithelial cells to the four *Candida* species (Fig. 4a). Since type I IFN responses are implicated in antiviral host defence, additional metagenomic analyses were performed and no viral contamination was detected.

The connection between ISG expression and mitochondrial functions of the host was characterized during early *Candida* infection. Morphological changes of the mitochondrial network in epithelial cells were observed, changing from reticular (uninfected) to fragmented (infected), and an accumulation of mitochondria around the nucleus (Fig. 4b). Some mitochondria in infected epithelial cells lost their integrity and changed their shape but not in uninfected cells (Fig. 4c,d). Additionally, endoplasmic reticulum regions surrounded these altered mitochondria, suggesting mitophagy of damaged mitochondria. Interestingly, mitochondria were also localized frequently around the invading hyphae of *C. albicans* (Fig. 4c).

Mitochondrial membrane potential ( $\Delta\Psi_m$ ), a key indicator of mitochondrial health, indicated depolarization in epithelial cells infected with any of the four species (Fig. 4e). This change in  $\Delta\Psi_m$  is associated with the production of mitochondrial reactive oxygen species (mtROS), which are critical players in the regulation of immune signalling pathways<sup>30</sup>. Epithelial mtROS levels were increased on infection with all four species (Fig. 4f). Finally, release of mitochondrial DNA (mtDNA) into the cytosol was observed during infection with all *Candida* species (Fig. 4g). The release of mtROS and mtDNA was not detected with killed *C. albicans* cells or when contact was restricted using a transwell system (Fig. 4e,f). This supports our notion that viable *Candida* cells in direct contact with epithelial cells induce mitochondrial dysfunctions at both transcriptional and biochemical levels (Fig. 4h).

During infection with bacteria or viruses, host mitochondria can release mtDNA into the cytosol acting as a damage-associated molecular pattern (DAMP) that activates immune pathways<sup>31</sup>. Cytosolic mtDNA can bind the DNA sensor cyclic GMP-AMP synthase and promote stimulator of interferon genes (STING)-IRF3-dependent signalling to induce a type I IFN response<sup>28</sup>. In line with this, depletion of epithelial mtDNA (Fig. 5a) prevented upregulation of ISGs after *Candida* infections (Fig. 5b). In addition, transfection of uninfected epithelial cells with amplified mtDNA induced ISG expression (Fig. 5c). Transfection of uninfected epithelial cells with total DNA from epithelial cells only induced ISGs when the transfected DNA contained mtDNA (Fig. 5d), which supports the role of mtDNA in the induction of ISG expression (Fig. 5e).

Although mitochondrial dysfunction is a hallmark of cellular apoptosis, no apoptotic or necrotic epithelial cells were observed

during the early stages of infections (Extended Data Fig. 5). This was expected since mitochondrial dysfunctions were only transiently observed. Later during infection, we observed necrotic cell death but no increase in apoptosis compared to the uninfected control (Extended Data Fig. 5). The A-431 cell line lacks functional p53, an important apoptosis inducer<sup>32</sup>. However, we observed similar mitochondrial depolarization in primary vaginal cells on *Candida* infections, while apoptosis levels did not differ between infected and uninfected cells (Extended Data Fig. 5). Additionally, treatment of A-431 cells with the apoptosis inducer staurosporine excluded that the observed mitochondrial signalling and induction of ISG expression were related to apoptosis (Extended Data Fig. 5).

The function of many ISGs is poorly characterized but induction is associated with protection against viral infections<sup>33</sup>. To gain insights into their role during *Candida* infection, selected ISGs (*IFI6*, *MX2*, *CMPK2*) were silenced in epithelial cells before infection with *C. albicans*. *IFI6* was selected since it was previously observed to be induced by *C. albicans*<sup>34</sup>, *MX2* was among the most highly upregulated common genes (this study) and *CMPK2* encodes a protein with mitochondrial localization<sup>35</sup>. The level of epithelial damage was increased once these ISGs were silenced (Fig. 6a). While stimulation of cells with IFN- $\beta$  (0.1 ng ml<sup>-1</sup>) before infection resulted in reduced damage (Fig. 6b); blocking IFN- $\alpha/\beta$  receptor (IFNAR) signalling led to increased damage (Fig. 6b). These data illustrate that type I IFN signalling increases epithelial resistance to *Candida* infection.

Neutrophil recruitment and activation is a hallmark of vaginal candidiasis<sup>36</sup>. Pro-inflammatory mediators, such as IL-6 or IL-1 $\beta$ , which are characteristic for these events, were not produced during *Candida* infection (Fig. 6c), while IL-1 $\alpha$  and IL-8 levels increased (Fig. 6d), which correlates with the level of damage. IL-8 levels also increased on IFNAR blocking (Fig. 6d), suggesting a relationship between epithelial type I IFN signalling and the initiation of pro-inflammatory responses, which can drive immunopathology in VVC.

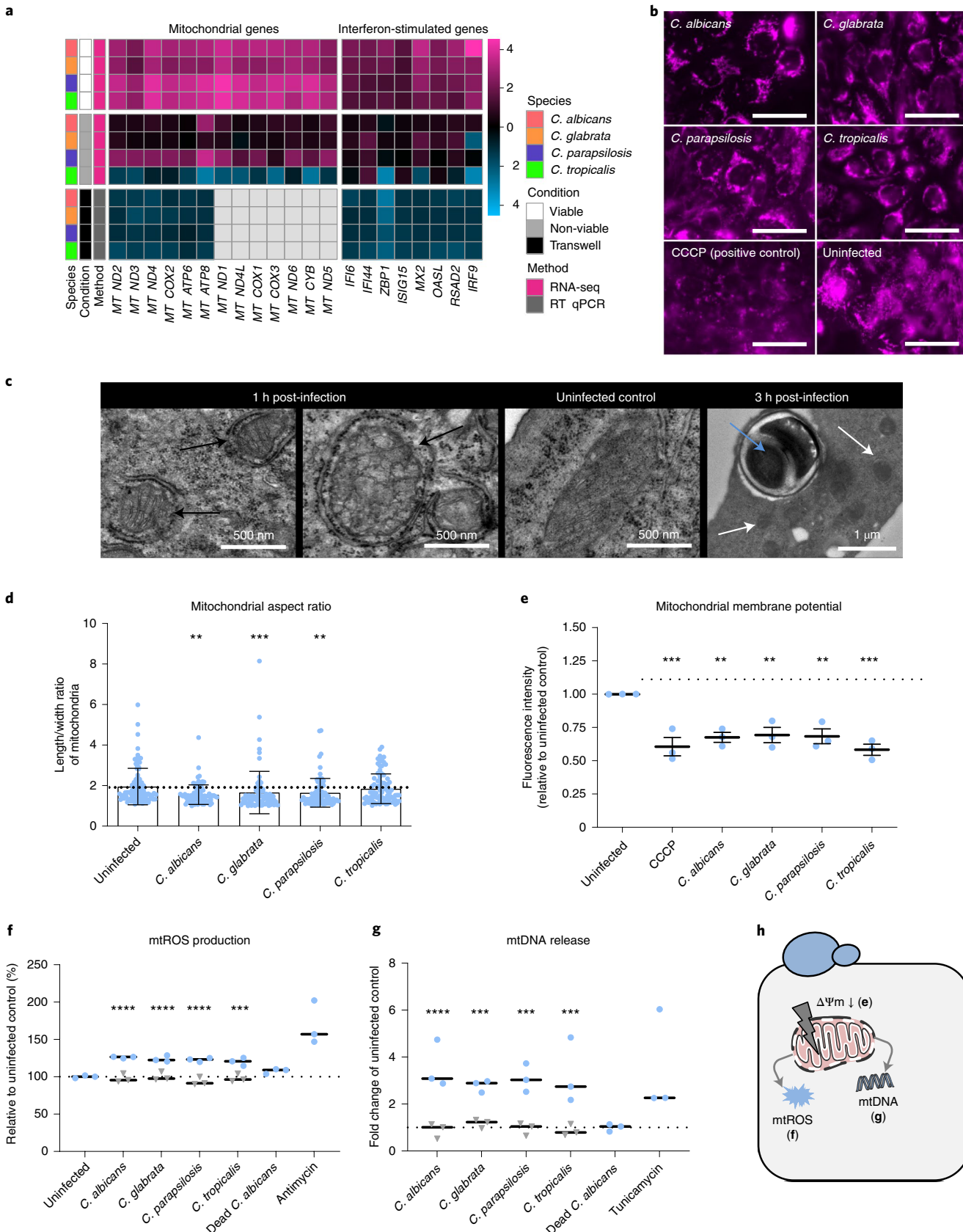
When exposing neutrophils to the culture supernatants of epithelial cells infected with *Candida* species, IL-8 release was observed (Fig. 6e). IL-8 levels further increased when the IFNAR receptor was blocked in the same setting (Fig. 6e). This suggests that type I IFN signalling in epithelial cells restricts pro-inflammatory responses and subsequent neutrophil activation (Fig. 6f).

**Damage-driven transcriptional responses.** While the initial phases of infection showed a conserved epithelial response, this response separated into different trajectories at later stages. Considering that host cell damage is a major determinant of pathogenicity<sup>37-39</sup>, we hypothesized that *Candida* species-specific differences in the damaging potential (Fig. 1 and Extended

**Fig. 4 | *Candida* species induce mitochondrial responses in vaginal epithelial cells.** **a**, Expression of mitochondrial and interferon-stimulated genes with all four species in direct contact with epithelial cells, with non-viable *Candida* cells, and in the transwell system. Data for infection in direct contact and with non-viable *Candida* cells were derived from RNA-seq data ( $\log_2(\text{fold change}) > 1.5$  for *C. albicans*, *C. glabrata* and *C. parapsilosis*;  $\log_2(\text{fold change}) > 1.3$  for infections with *C. tropicalis*), while transwell experiments were done additionally as  $n=3$  independent experiments; transcription levels were analysed using RT-qPCR. **b**, Mitochondrial imaging by fluorescence microscopy using MitoTracker Deep Red FM at 1 h post-infection. Scale bars, 50  $\mu\text{m}$ . **c**, TEM analysis of mitochondria in uninfected and *C. albicans*-infected epithelial cells (1 and 3 h post-infection): loss of mitochondrial integrity in infected epithelial cells (white arrows); mitochondria (black arrow) localized around the invading hyphae of *C. albicans* (blue arrow) at 3 h post-infection. **d**, Mitochondrial aspect ratio quantified by TEM at 1 h post-infection ( $n \geq 80$  mitochondria examined over 1 independent experiment). **e**, Mitochondrial membrane potential change at 1 h post-infection (positive control 100  $\mu\text{M}$  of CCCP). **f**, Levels of mtROS production at 1 h post-infection (positive control 100  $\mu\text{M}$  of antimycin). **g**, Levels of mtDNA released into the cytosol (qPCR) on infection with *Candida* species at 6 h post-infection (positive control 10  $\mu\text{M}$  of tunicamycin). **h**, Schematic model of the events associated with mitochondrial dysfunctions resulting in mtROS production and mtDNA release. All data are derived from  $n=3$  independent experiments, unless indicated otherwise (d). Representative microscopy images (b-c) were taken from  $n=3$  biological replicates and similar results were observed. All values are presented as the mean  $\pm$  s.d. relative to the uninfected (-) control (dotted lines on (d-g)). Statistical significance is indicated as \* $P \leq 0.05$ , \*\* $P \leq 0.01$ , \*\*\* $P \leq 0.001$ , \*\*\*\* $P \leq 0.0001$  (Kruskal-Wallis test with two-sided Dunn's multiple comparison (d) and one-way ANOVA with Dunnett's multiple comparisons test (e-g)). Credit: graphics in h adapted from Servier under a Creative Commons licence CC BY 3.0.

Data Fig. 6), reflected by the pattern observed in the PCA plot (Fig. 3d), drive the different transcriptional responses during late infection.

Epithelial cell damage during *C. albicans* infection is mediated by the cytolytic toxin candidalyisin<sup>40,41</sup>. Deletion of the *ECE1* gene, which encodes candidalyisin, renders *C. albicans* almost unable to



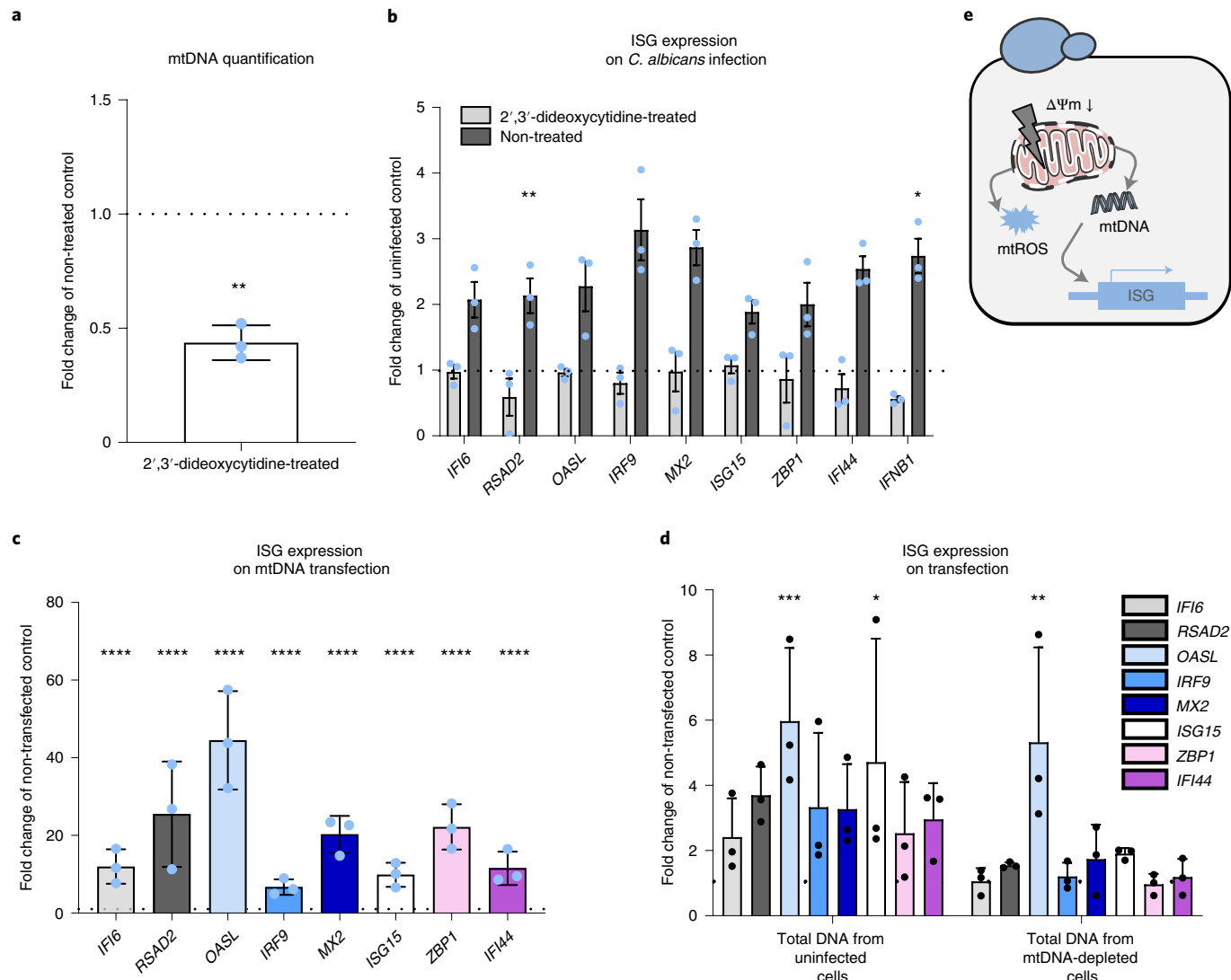


**Fig. 5 | Role of mtDNA in the induction of type I IFN in vaginal epithelial cells.** **a**, Depletion of mtDNA level by treatment of vaginal epithelial cells with 2',3'-dideoxycytidine for 6 d, measured by qPCR. **b**, Relative expression (RT-qPCR) of selected ISGs (IFNB1, IFI6, RSAD2, OASL, IRF9, MX2, ISG15, ZBP1 and IFI44) in *C. albicans*-infected, mtDNA-depleted epithelial cells at 3 h post-infection. **c**, Relative expression (RT-qPCR) of selected ISGs on transfection of epithelial cells with amplified mtDNA fragments at 6 h post-transfection. **d**, Relative expression of selected ISGs (RT-qPCR) in epithelial cells transfected with total DNA obtained from vaginal epithelial cells with and without mtDNA depletion at 6 h post-transfection. **e**, Schematic model of ISG expression induction by released mtDNA. All values are presented as the mean  $\pm$  s.d. relative to the uninfected/non-transfected (—) control (dotted lines) of  $n=3$  independent experiments. Statistical significance is indicated as \* $P \leq 0.05$ , \*\* $P \leq 0.01$ , \*\*\* $P \leq 0.001$ , \*\*\*\* $P \leq 0.0001$  (two-tailed one-sample t-test (a), two-way ANOVA and Sidak's multiple comparisons test (b,d) and one-way ANOVA with Dunnett's multiple comparisons test (c)). Credit: graphics in e adapted from Servier under a Creative Commons licence CC BY 3.0.

inflict damage to epithelial cells, despite normal growth, adhesion, filamentation and invasion properties<sup>25,40</sup>.

To determine whether candidalysin-driven epithelial cell damage might dictate the transcriptional response of epithelial cells, the transcriptional response on interaction with the *C. albicans* *ece1Δ/Δ* mutant was investigated. The epithelial transcriptional response to the candidalysin-deficient mutant was notably similar to the response to the non-damaging species *C. parapsilosis* (Extended Data Figs. 6 and 7). This confirms a pivotal role for host cell damage as the major driver of epithelial transcriptional responses to *Candida* infections. GO term enrichment analysis of 774 genes, specifically upregulated on exposure to damaging wild-type *C. albicans*, showed no significant enrichment for any process. However, previous studies demonstrated that candidalysin induces c-Fos and mitogen-activated protein kinase-driven release

of the pro-inflammatory cytokines IL-1 $\alpha$  and IL-1 $\beta$  and the chemokine IL-8 in vaginal epithelial cells<sup>12,25</sup>. Manual inspection revealed similar responses including upregulation of *HBEGF*, *CXCL1*, *CXCL2*, *IL1A*, *IL1B*, *CXCL8* and *CSF2* and genes associated with the ‘danger’ response pathway *FOS*, *JUN* and *DUSP1* (refs. 12,25). This confirms that epithelial damage and pro-inflammatory signals that drive neutrophil recruitment induced by *C. albicans* depend almost exclusively on candidalysin.

## Discussion

In this study, we dissected the interaction of the main four *Candida* species that cause VVC with human vaginal epithelial cells. Large-scale dual transcriptomic analysis of human and fungal cells during the course of infection revealed common and species-specific *Candida* pathogenicity patterns. We observed a

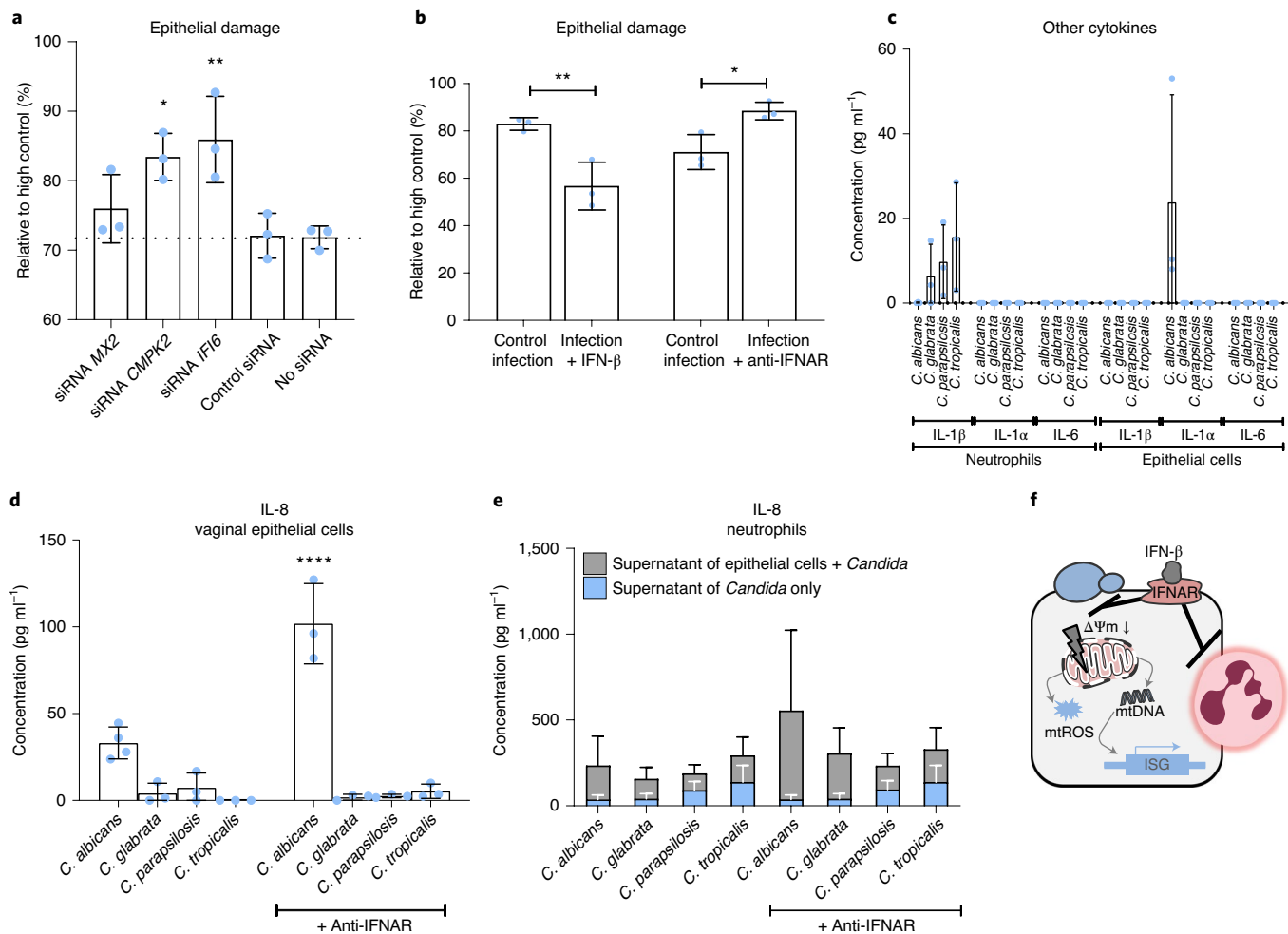


**Fig. 6 | Type-I IFN signalling increases epithelial resistance and suppresses innate immune activation.** **a**, Epithelial damage caused by *C. albicans* 24 h post-infection after RNA interference for selected ISGs (*MX2*, *CMPK2*, *IFI6*). Transfection with control siRNA, consisting of a scrambled sequence that will not lead to the specific degradation of any mRNA, was used as a control (dotted line). **b**, Epithelial damage caused by *C. albicans* 24 h post-infection without and with 0.1 ng ml $^{-1}$  of IFN- $\beta$  and the addition of anti-IFNAR antibody. **c**, Levels of IL-6, IL-1 $\beta$  and IL-1 $\alpha$  secretion by neutrophils incubated with supernatants from infected epithelial cells and by epithelial cells infected with *Candida* species 24 h post-infection. **d**, Levels of IL-8 secretion by infected epithelial cells 24 h post-infection with or without the addition of anti-IFNAR antibody. **e**, Levels of IL-8 secretion by neutrophils after 24-h incubation with supernatants from epithelial cell infections with or without the addition of an anti-IFNAR antibody. Control supernatants of *Candida* cells alone were included to ensure that the neutrophils responded to secretions of epithelial cells rather than the fungus (blue bars). **f**, Schematic model of the proposed role of the type I IFN pathway in immune regulation and protection against *Candida* infection. All values are presented as the mean  $\pm$  s.d. of  $n=3$  independent experiments (except  $n=4$  for IL-8 production by epithelial cells on *C. albicans* infection). Statistical significance is indicated as  $*P \leq 0.05$ ,  $**P \leq 0.01$ ,  $***P \leq 0.0001$  (one-way ANOVA with Dunnett's multiple comparisons test (**a**) or Tukey's multiple comparisons test (**b,d**)). Credit: graphics in **f** adapted from Servier under a Creative Commons licence CC BY 3.0.

biphasic host response to *Candida* species, which is characterized by an early common mitochondria-induced type I IFN signalling and diverged responses at later stages depending on the species-specific capacities to inflict damage to the vaginal epithelial cells.

It has previously been hypothesized that phylogenetically diverse *Candida* species independently acquired their ability to colonize and infect humans and thus are expected to use distinct sets of pathogenicity mechanisms<sup>6,23</sup>. Our study empirically supports this hypothesis by showing that the main VVC pathogens express species-specific transcriptional responses and pathogenicity patterns on contact with vaginal epithelial cells, even when only orthologous genes were considered.

Similarly, the epithelial transcriptional responses at the late stages of infection were specific depending on the *Candida* species. These diverse patterns paralleled the varying damaging capacities of the four *Candida* species. We confirmed fungal-induced damage as

the major driver of epithelial responses by infecting epithelial cells with the non-damaging candidalysin-deficient *C. albicans ece1* $\Delta/\Delta$  mutant. The epithelial transcriptional response to this mutant did not resemble the response to wild-type *C. albicans*, but instead was similar to the response to the non-damaging species *C. parapsilosis* at the late stages of infection. This finding confirms the crucial role of candidalysin during interaction of *C. albicans* with vaginal epithelial cells leading to DAMP release that can catalyse immunopathology during vaginal infections<sup>25</sup>.

In contrast, the epithelial response towards the different *Candida* species was highly uniform at the early stages. This initial response was driven by common epithelial processes rather than by convergent activities (such as virulence programmes) of the tested *Candida* species. For example, independent of their viability, *DOCK8* expression was upregulated after infection with any of the four *Candida* species (Supplementary Files 5–8). Although *DOCK8* has multiple

signalling functions, it was suggested that it promoted immune responses to diverse external stimuli<sup>42</sup>. Several studies associated *DOCK8* with mucocutaneous candidiasis due to impaired T<sub>H</sub>17 differentiation<sup>43–45</sup>. Thus, it is tempting to speculate that *DOCK8* may regulate the recognition of *Candida* species by epithelial cells.

Mitochondria-encoded genes and genes associated with the type I IFN response pathway were uniformly upregulated. While type I IFN responses are associated with viral infections<sup>46</sup>, type I IFN responses have been observed in peripheral blood mononuclear cells infected with *C. albicans*<sup>34</sup>. Additionally, type I IFN responses were recently shown to dysregulate host iron homeostasis and enhance *C. glabrata* infection<sup>47</sup>; the type I IFN-inducing RIG-I helicase MDA5 has been associated with systemic and chronic mucocutaneous candidiasis<sup>48</sup>. Finally, IFN $\alpha$ R1 signalling is crucial for efficient host defence against systemic candidiasis in mice<sup>49</sup>.

Our data show that type I IFN signalling, induced by vaginal epithelial cells in response to *Candida* species, increases epithelial resistance to infection and dampens pro-inflammatory responses.

Such an immune response may be relevant in host niches colonized by commensal microbes that need to be tolerated without induction of inflammation. For example, intestinal epithelial cells regulate the durability and specificity of immune responses and guide the immune system to differentiate between commensal and pathogenic microbiota via expression of type I IFN and ISGs<sup>50–52</sup>. Since *Candida* species are commensals of the vaginal mucosa<sup>53</sup>, the epithelial type I IFN pathway may maintain the threshold between commensalism and pathogenicity and regulate antifungal immunity. Our results show a protective role for ISGs and IFNAR signalling in increasing epithelial resistance to *Candida*-induced damage while reducing potentially detrimental pro-inflammatory responses. Supporting this, Li et al.<sup>54</sup> showed that administration of human IFN $\alpha$ -2b decreased the inflammation and vaginal epithelial damage in a rat VVC model. The combined effects, immunomodulation and epithelial antifungal resistance, may be crucial to restrict *Candida* species to commensalism and avoid inflammation-driven pathology. Moreover, this highlights the type I IFN response as a potential target for host-directed therapy aimed at improving epithelial resistance and preventing immunopathology. Such a therapy could benefit VVC patients that fail to recover with antifungal treatment alone, a phenomenon often observed in women with recurrent VVC<sup>55</sup>.

At the early infection stage, genes encoded by mtDNA, in particular genes coding for the respiratory electron transport chain, were upregulated. Apart from the well-established roles in metabolism and energy production, mitochondria are central hubs in innate immunity<sup>26,27</sup>. Mitochondrial dysfunction, resulting in mtROS and mtDNA release into the cytosol, can act as a DAMP and activate various signalling pathways<sup>26–28,56–58</sup>, including induction of cytokine production<sup>59</sup> and type I IFN responses<sup>60</sup>. Intriguingly, altered mitochondrial function at the early stages of infection were observed in different host cell types on infections with various bacterial pathogens<sup>61–64</sup>, including *Chlamydia trachomatis*<sup>65</sup>, *Chlamydia pneumoniae*<sup>66</sup>, *Listeria monocytogenes*<sup>67</sup> and the parasite *Toxoplasma gondii*<sup>68</sup>. However, these mechanisms have not yet been observed during fungal infections. We observed that mitochondria in *Candida*-infected vaginal epithelial cells changed shape and lost integrity, had decreased membrane potential and released mtROS and mtDNA. The release of mtDNA was observed to act as a DAMP that activates the type I IFN pathway during *Candida* infections of the vaginal epithelium. This activation may potentially occur through the STING pathway, as shown previously for *Streptococcus pneumoniae*<sup>69</sup>, at the level of post-translational modifications<sup>70</sup>.

To maintain epithelial integrity and mount an effective epithelial host defence while preventing detrimental inflammatory responses, such a mitochondrial response must occur on a sublethal level<sup>59</sup>. Accordingly, no changes in apoptosis were observed over the

course of infection. The non-lethal mitochondrial dysfunction was also independent of necrosis, which was only observed at the later stages. Likewise, we observed consistent activation of the type I IFN pathway, which is suppressed by apoptotic caspases<sup>71</sup>. Consequently, induction of apoptosis abrogated expression of ISGs. Similar studies with *L. monocytogenes* and *T. gondii* showed that mitochondrial dysfunction was uncoupled from the apoptotic pathway<sup>67,68</sup>. During infection of epithelial cells with diverse microbes, the mitochondrial apoptosis apparatus can be activated at a low level, which is insufficient to induce apoptosis<sup>59,72</sup>. This phenomenon has been termed limited mitochondrial outer membrane permeabilization (MOMP), or ‘minority MOMP’, and induces pro-inflammatory cytokine production via STING.

Viruses, bacteria and parasites can induce minority MOMP, thereby contributing to cytokine release during infection<sup>59</sup>. We propose that this mechanism plays a significant role in epithelial sensing of *Candida* species, induction of epithelial antifungal immunity and modulation of immune responses via type I IFN signalling.

It remains to be determined how *Candida* species initiate the mitochondria-induced epithelial type I IFN response. We observed mitochondrial signalling at stages when *C. albicans* had not yet invaded or damaged epithelial cells, whereas all other *Candida* species failed to invade epithelial cells. Therefore, we propose that the induction of mitochondrial signalling may rely on sensing of pathogen-associated molecular patterns (PAMPs).

In summary, we identified species-specific pathogenicity patterns of *Candida* species infecting vaginal epithelial cells, which are reflected at the transcriptional level during the course of infection. In contrast, vaginal epithelial cells exhibit a conserved response at early stages, but a diverse, damage-driven response at later stages. The conserved response was characterized by non-lethal mitochondrial signalling, which induced a type I IFN response that protects against *Candida*-induced damage and modulates pro-inflammatory responses. This acts as a common pathway of host-pathogen interactions between vaginal epithelial cells and *Candida* pathogens.

## Methods

**Fungal strains and culture conditions.** *C. albicans* SC5314 (ref. <sup>73</sup>), *Candida glabrata* ATCC 2001 (obtained from ATCC), *C. tropicalis* DSM 4959 (obtained from the German Collection of Microorganisms and Cell Cultures), *C. parapsilosis* 73-037 (ref. <sup>74</sup>) and *C. albicans* *ee1* $\Delta/\Delta$ <sup>40</sup> were used in this study. For all experiments, single colonies were picked from yeast extract peptone dextrose (YPD) agar plates and grown overnight in liquid YPD medium in an orbital shaker at 180 r.p.m. at 30 °C (*C. albicans*, *C. tropicalis* and *C. parapsilosis*) or 37 °C (*C. glabrata*). Yeast cells were then collected by centrifugation (20,000g, 1 min), washed twice with PBS and adjusted to 2 × 10<sup>6</sup> yeast cells per ml<sup>-1</sup>.

**In vitro vaginal epithelial infection model.** To mimic the vaginal epithelium, A-431 epithelial cells (ACC 91) were used. These cells are derived from a vulva epidermoid carcinoma and routinely used to model the vaginal mucosa<sup>75,76</sup>. A-431 cells were authenticated using short tandem repeat analysis (DNA fingerprinting) and routinely tested for the absence of *Mycoplasma* contamination. Epithelial cells were cultivated in Roswell Park Memorial Institute (RPMI) 1640 medium (Thermo Fisher Scientific) supplemented with 10% fetal calf serum (FCS; Bio&SELL) in a humidified incubator at 37 °C and 5% CO<sub>2</sub>. For infection, epithelial cells were seeded in 6-well plates (3 × 10<sup>5</sup> cells per well) and cultured for 2 d. On the day of infection, the medium in each well was replaced with 1.5 ml of RPMI 1640 without FCS and incubated for 30 min to allow cells to adjust to the change of medium. In subsequent bioinformatics analyses, we considered the control samples at 30 min in this medium as the 0 h time point. Epithelial cells were subsequently infected with *Candida* cells (1.5 ml of 2 × 10<sup>6</sup> yeast ml<sup>-1</sup> in RPMI 1640 without FCS) and incubated at 37 °C and 5% CO<sub>2</sub>. Samples for RNA isolation were collected at different time points: 3, 12 and 24 h post-infection. More specifically, the well content was removed and replaced with 500 μl of RLT buffer (QIAGEN), containing 1% β-mercaptoethanol (Roth). Cells were detached using a cell scraper (<3 min), immediately shock-frozen in liquid nitrogen and stored at –80 °C until further use (see ‘RNA isolation and pooling’). As controls, *Candida* cells alone and epithelial cells alone were incubated for 30 min (0 h control: C0) and 24 h (24 h control: C24) and samples for RNA isolation were collected as described above.

**RNA isolation and pooling.** Collected samples were defrosted on ice and centrifuged for 10 min (20,000g, 4 °C). The supernatant was transferred to a

new microcentrifuge tube and used to isolate human RNA (RNeasy Mini Kit; QIAGEN), according to the manufacturer's instructions. Fungal RNA was isolated from the pellet using a freezing–thawing method, as described previously<sup>77</sup>. Both human and fungal RNA concentrations were quantified using a NanoDrop 1000 Spectrophotometer (Thermo Fisher Scientific) and RNA quality was assessed with an Agilent 2100 Bioanalyzer (Agilent Technologies). To subsequently achieve sufficient sequencing depth of both counterparts for a robust differential gene expression analysis<sup>78</sup>, corresponding fungal and human RNA samples were pooled in a 2:3 ratio by weight for further library preparation and sequencing. Before pooling, we first checked whether this strategy would result in ambiguous read mappings between the host and pathogen data after sequencing and data analysis. To assess the rates of cross-mapping, that is, reads originated from human but mapped to fungi and vice versa, which can bias expression level quantifications, we used CROSSLAPPER v1.1.0 (ref. <sup>79</sup>), which simulates reads from multiple reference genomes/transcriptomes, maps the data back to the concatenated reference sequences and reports the rates of cross-mapping. We used the 'RNA' mode of CROSSLAPPER and simulated and back-mapped 20 and 40 million 2×50 and 2×75 reads for each fungal species and human, respectively. In all cases, the pooling and sequencing strategy resulted in virtually no cross-mapping between human and yeast data (Supplementary Files 1–4).

**Growth curves.** *Candida* cells were adjusted to 10<sup>6</sup> yeast ml<sup>-1</sup> either in YPD or RPMI medium. Growth was monitored in 96-well-plates by measuring the absorbance at 600 nm every 30 min for 24 h at 37 °C in a microplate reader (Tecan M-Plex). Before each measurement, plates underwent 10-s orbital shaking followed by 10-s waiting time. The OD<sub>600</sub> values were converted into log<sub>2</sub> and the generation time was calculated from the slope of the exponential growth phase. The experiment was repeated five times.

**Ultraviolet killing of *Candida*.** *Candida* cells from overnight cultures were collected by centrifugation, washed twice with PBS and adjusted to approximately 5×10<sup>7</sup> yeast ml<sup>-1</sup> in PBS. The suspension was transferred to a Petri dish as a thin liquid layer (10 ml) and exposed to 4 doses of 100–120 mJ per cm<sup>2</sup> in an ultraviolet (UV) CROSSLINKER (CL 508S; Uvitec). The efficiency of UV killing was evaluated by plating 50 µl of the sample onto YPD agar and incubated for 48 h at 30 °C.

**Adhesion assay.** Epithelial cells were infected with *Candida* yeast cells as described above and incubated for 1 h. Non-adherent *Candida* cells were removed by rinsing with PBS. Subsequently, epithelial cells with adhered *Candida* were fixed with Roti Histofix 4% (Roth). Adherent *Candida* cells were stained with Alexa Fluor 647 conjugate of succinylated concanavalin A (Invitrogen) and visualized using a fluorescence microscope (Leica DM5500B; Leica DFC360 FX). Pictures of each sample were taken until a total of 100 adherent cells were counted. Adhesion was calculated based on the average of *Candida* cells counted in each picture with a defined area. This number was expressed as a percentage of adhered cells versus inoculated cells<sup>77</sup>.

**Invasion assay and hyphal length.** Epithelial cells were infected with *Candida* cells as described above and incubated for 3 h. Non-adherent *Candida* cells were removed by rinsing with PBS and samples were fixed with Roti Histofix 4%. Extracellular, non-invasive fungal components were stained by concanavalin A. After rinsing with PBS, epithelial cells were permeabilized in 0.5% Triton X-100 for 10 min. Next, fungal cells were stained with Calcofluor white (Sigma-Aldrich) and visualized by fluorescence microscopy. The total hyphal length was noted as well as the percentage of invasive hyphae (only Calcofluor white-stained), counted from at least 100 hyphae per strain for each biological replicate.

**Epithelial damage assay.** Epithelial cells were infected with *Candida* cells as described above and incubated for 24 h. Release of the cytoplasmic enzyme lactate dehydrogenase (LDH) was measured as a marker for necrotic epithelial damage<sup>80</sup> using a Cytotoxicity Detection Kit (Roche) according to the manufacturer's instructions. The background LDH value of uninfected epithelial cells (low control) was subtracted and the corrected LDH release was expressed as the percentage of high (full lysis) control (maximum LDH release induced by the addition of 0.25% Triton X-100 to uninfected epithelial cells for 5 min) unless otherwise stated. For the protection effect experiments, 0.1 ng ml<sup>-1</sup> of IFN-β (InvivoGen) or neutralizing anti-human IFNAR2 antibody (4 ng ml<sup>-1</sup>; PBL InterferonSource) were added to epithelial cells 3 h before infection.

**Transwell assay.** Epithelial cells were seeded in 24-well plates (1×10<sup>5</sup> cells per well) in RPMI 1640 with FCS and incubated for 2 d at 37 °C and 5% CO<sub>2</sub>. After medium exchange with 750 µl of RPMI 1640 without FCS, transwell inserts (polycarbonate membrane inserts with 0.4 µm pore size; Corning), loaded with 250 µl of *Candida* suspension (4×10<sup>6</sup> yeast ml<sup>-1</sup>), were placed in the wells. After 3 h of incubation, the inserts were discarded and human RNA samples were collected and isolated as described above.

**RT-qPCR.** Isolated RNA (500 ng) was treated with DNase I (Fermentas) according to the manufacturer's recommendations and subsequently transcribed

into complementary DNA using 0.5 µg of Oligo(dT)<sub>12–18</sub> Primer, 200 U of Superscript III Reverse Transcriptase and 40 U of RNaseOUT Recombinant RNase Inhibitor (Thermo Fischer Scientific). The cDNA obtained was diluted 1:5 and used for qPCR with the GoTaq qPCR Master Mix (Promega Corporation) in a CFX96 thermocycler (Bio-Rad Laboratories). The expression levels were normalized against β-actin or 18S ribosomal RNA. All primers used are listed in Supplementary Table 2.

**Measurement of epithelial cell mtDNA release.** The release of mtDNA in response to infection was measured using the protocol of Bronner and O'Riordan<sup>81</sup> with some modifications. Briefly, epithelial cells were seeded in 6-well plates and infected as described above. After 6 h of infection, the medium and non-adherent *Candida* cells were removed. After the addition of 200 µl of the cell membrane detergent IGEPAL CA-630 (1%, NP-40; Sigma-Aldrich), cells were loosened by scraping. Lysates were incubated on ice for 15 min and centrifuged (12,000 g, 15 min, 4 °C). The supernatant was used to isolate human mtDNA from the cytosolic fraction using the DNeasy Blood & Tissue Kit (QIAGEN), according to the manufacturer's instructions. Finally, cytosolic human mtDNA was measured by qPCR using 18S rRNA as a reference<sup>81</sup>. Results are presented relative to an uninfected control. Tunicamycin (10 µM; Sigma-Aldrich) was used as a positive control, as an endoplasmic reticulum stress inducer that leads to mitochondrial dysfunction<sup>82</sup>. The same procedure was carried out on yeast cells only to exclude that fungal cells would also release mtDNA following this protocol. The lysis step did not cause any lysis of yeast cells and no DNA was detected after the isolation procedure, confirming that the DNA obtained from the infected epithelial cells originated from epithelial cells only.

**Measurement of ΔΨm.** The ΔΨm was assessed using the dye MitoTracker Deep Red FM (Thermo Fisher Scientific, excitation (Ex)/emission (Em) = 644/665 nm). Epithelial cells were seeded and infected in 6-well plates and stained with 20 nM of MitoTracker Deep Red FM for 15 min at 37 °C. Epithelial cells were then detached using Accutase and fixed with Roti Histofix 4%. Fluorescence was quantified by flow cytometry (BD FACSVerso; BD Biosciences), counting 10,000 events; the data were collected using the BD FACSuite v1.0.6.5230 software and analysed with FlowJo v10.2. Carbonyl cyanide 3-chlorophenylhydrazone (CCCP), a protonophore that causes mitochondrial depolarization, was used as a positive control (100 µM).

**Epithelial cell mtROS detection.** Production of mtROS was measured using a Mitochondrial Reactive Oxygen Species Detection Assay Kit (Cayman Chemical). Epithelial cells were seeded and infected in a black clear-bottom 96-well plate; measurement of mtROS production of infected and uninfected cells was done at 1 h post-infection according to the manufacturer's instructions. Antimycin A (100 µM), which induces superoxide radicals leakage from mitochondria, was used as a positive control.

**RNA interference assay.** The RNA interference assay was used to silence the expression of selected ISGs (*IFI6*, *MX2* and *CMPK2*). Small interfering RNA, control siRNA (siRNA-A; catalogue no. sc-37007), siRNA transfection reagent and siRNA transfection medium were purchased from Santa Cruz Biotechnology. Epithelial cells were seeded in a 6-well plate and transfected with 1 µg of siRNA according to the manufacturer's instructions. After 48 h, cells were infected with *C. albicans*; 3 h post-infection, RNA was isolated and silencing of selected genes was confirmed using RT-qPCR. LDH release was measured 24 h post-infection.

**mtDNA depletion assay.** Epithelial cells were seeded in 6-well plates and incubated for 2 d. Once confluent, 200 µM of 2',3'-dideoxyctydine (Jena Bioscience) was added to the medium and epithelial cells were incubated for 6 d. mtDNA depletion was confirmed by quantifying mtDNA using qPCR, as described above.

**Transfection of epithelial cells.** MtDNA was PCR-amplified from the entire human mitochondrial genome in 17 overlapping fragments as described previously<sup>83</sup>. Epithelial cells were transfected with amplified mtDNA fragments (Fig. 5c) or total DNA isolated from epithelial cells with and without their mtDNA depleted (Fig. 5d). Total DNA was isolated using the DNeasy Blood & Tissue Kit. A total of 2 µg ml<sup>-1</sup> of DNA was used to transfet epithelial cells using the UltraCruz Transfection Reagent (Santa Cruz Biotechnology) according to the manufacturer's instructions. After 6 h, RNA samples were collected and the expression of ISGs was quantified by RT-qPCR.

**Apoptosis/necrosis assay.** Epithelial cells were seeded in black 96-well plates and infected with *Candida* cells as described above. At 3 and 24 h post-infection, epithelial cells were stained for apoptotic (Apopxin Green Indicator, Ex/Em = 490/525 nm), necrotic (7-aminoactinomycin D, Ex/Em = 546/647 nm) and healthy cells (CytoCalcein Violet 450, Ex/Em = 405/450 nm) using the Apoptosis/Necrosis Assay Kit (Abcam). Fluorescence was measured in a microplate reader (Tecan M-Plex). Staurosporine (1.2 µM; Sigma-Aldrich) was used as a positive control, while uninfected epithelial cells were used as a negative control.

**Apoptosis induction.** Epithelial cells were seeded in 96-well plates and infected with *Candida* as described above with the addition of staurosporine (1.2 µM) simultaneously with infection. After 6 h, RNA samples were collected and the expression of ISGs was quantified by RT-qPCR. Results were compared to infected cells incubated in the medium without staurosporine.

**Collection of epithelial cell supernatants.** Epithelial cells were infected with *Candida* cells as described above and incubated for 24 h in the presence or absence of neutralizing anti-human IFNAR2 antibody. Supernatants were collected and stored at -80°C until use (see Methods sections 'Cytokine release' and 'Neutrophil cytokine production'). The supernatants of only *Candida* cells grown in the absence of epithelial cells were included as control.

**Cytokine release.** Epithelial cells were infected with *Candida* cells as described above and incubated for 24 h. The release of IL-6, IL-8, IL-1 $\alpha$  and IL-1 $\beta$  was measured with commercially available human enzyme-linked immunosorbent assay kits (IL-6, IL-8, IL-1 $\beta$ , Invitrogen; IL-1 $\alpha$ , R&D Systems) according to the manufacturers' instructions.

**Blood donors.** Human peripheral blood was collected from healthy volunteers ( $n=3$ ) with ethical approval and after obtaining written informed consent. This study was conducted according to the principles expressed in the Declaration of Helsinki version 2008. The blood donation protocol and use of blood for this study were approved by the institutional ethics committee of Jena University Hospital (permission no. 2207-01/08).

**Neutrophil cytokine production.** Primary human neutrophils were isolated from blood using a previously published protocol<sup>84</sup> and seeded in a 24-well plate ( $5 \times 10^5$  cells ml $^{-1}$ ). Neutrophils were exposed for 24 h to the supernatants of epithelial cells that had been infected with each of the *Candida* species (24 h post-infection) to determine whether pro-inflammatory mediators released by epithelial cells played a role in neutrophil stimulation. The control supernatants of *Candida* cells alone were included to ensure that the neutrophils responded to the secretions of epithelial cells rather than the fungus (blue bars on Fig. 6e). After incubation, cytokine release was measured using an enzyme-linked immunosorbent assay as described above.

**Fluorescence microscopy.** Epithelial cells were seeded in μ-Slide 8 Well (IBIDI) and infected with *Candida* cells as described above. At 1 h post-infection, epithelial cells were stained with 100 nM of MitoTracker Deep Red FM for 15 min at 37°C and washed and fixed with Roti Histofix 4%. Fluorescence imaging was done with the Cell Observer microscope (Carl Zeiss) with fluorescence settings at 644 and 665 nm. CCCP was used as a positive control (100 µM). Image acquisition was done in a fully blinded manner to avoid potential bias.

**Transmission electron microscopy and imaging.** Cells were fixed by adding glutaraldehyde (2.5% (v/v) final) to the growth medium. After 1 h, the cell layer was gently scraped off the surface, collected as a pellet by centrifuging at 600 g and washed three times with PBS. After fixation in osmium tetroxide (1% (w/v) in distilled water) for 1 h, dehydration in ascending ethanol series with post-staining in uranyl acetate was performed. Afterwards, samples were embedded in epoxy resin (Araldite) and sectioned ultrathin (60 nm) using an ultramicrotome (Leica Ultracut E; Leica Biosystems). After mounting on filmed copper grids and post-staining with lead citrate, the sections were studied in a transmission electron microscope (EM 902 A; ZEISS) at 80 kV. Images were acquired with a 1k FastScan CCD camera (TVIPS). The mitochondrial aspect ratio (the ratio of length/width) was measured using ImageJ version 1.43h by analysing at least 80 mitochondria for each condition<sup>85</sup> in 1 biological replicate. Irregular structures were excluded from analysis. All transmission electron microscopy (TEM) analyses were conducted in a fully blinded manner to avoid potential bias in image acquisition and analyses.

**Primary vaginal cells.** Primary human vaginal epithelial cells (catalogue no. PCS-480-010) were obtained from ATCC and cultured in vaginal epithelial cell basal medium (catalogue no. PCS-480-030; ATCC), supplemented with components from the Vaginal Epithelial Cell Growth Kit (catalogue no. PCS-480-040; ATCC). Cells were not authenticated but they were routinely checked for the absence of *Mycoplasma* contamination. Apoptosis/necrosis and mitochondrial membrane potential assays were performed as described for A-431 cells.

**RNA-seq library preparation and sequencing.** Library preparation for RNA-seq was performed with the TruSeq Stranded mRNA Sample Prep Kit v2 (catalogue no. RS-122-2101/2; Illumina) according to the manufacturer's instructions unless otherwise stated. One microgram of total RNA was used for poly(A)-mRNA selection using streptavidin-coated magnetic beads. Samples were then fragmented to approximately 300 base pairs (bp); subsequently, cDNA was synthesized using reverse transcriptase (SuperScript II; Invitrogen) and random primers. The second strand of the cDNA incorporated deoxyuridine triphosphate in place of deoxythymidine triphosphate. Double-stranded DNA was further used for library preparation. It was subjected to A-tailing and ligation of the barcoded TruSeq

adaptors. All purification steps were done using AMPure XP beads (Agencourt). Library amplification was performed by PCR on size-selected fragments using the primer cocktail supplied in the kit. Final libraries were analysed using the Agilent DNA 1000 chip (Agilent) to estimate the quantity and check fragment size distribution; they were then quantified by qPCR using the KAPA Library Quantification Kit (Kapa Biosystems) before amplification with Illumina's cBot. To avoid potential batch effects, all samples were randomly distributed on the sequencing flow cells.

Libraries were sequenced with 2 × 50 ( $n=21$ ), 2 × 75 ( $n=70$ ) and 2 × 150 ( $n=1$ ) read lengths on the Illumina HiSeq 2500 system (2 × 50 bp) and HiSeq 3000 (the rest) at the Genomics Unit of the Centre for Genomic Regulation, Barcelona, Spain. Samples that contained mixed fungal and human RNA were sequenced for (on average) almost equal to 65 million reads (Supplementary Table 1 and Extended Data Fig. 1) to achieve sufficient sequencing depth for robust downstream analysis<sup>78</sup>.

**Bioinformatics data analysis.** FastQC v.0.11.6 (ref. <sup>86</sup>) and MultiQC v.1.0 (ref. <sup>87</sup>) were used to perform the quality control of raw sequencing data. Read trimming, when necessary, was performed by Trimmomatic v.0.36 (ref. <sup>88</sup>) with TruSeq3 adaptors using the 2:30:10 parameters and discarding reads shorter than the sequenced read length.

For read mapping and quantification, we used the splice junction-sensitive read mapper STAR v.2.5.2b<sup>89</sup> using the basic two-pass mode and default parameters. For samples comprising either fungal or human RNA, reads were mapped to the corresponding reference genomes. In the case of pooled samples containing RNA from both host and pathogen, data were mapped to concatenated human and corresponding yeast reference genomes. For human data, we used the primary genome assembly GRCh38 and genome annotations from the Ensembl database release 89 (last accessed on 8 August 2017 (ref. <sup>90</sup>)). Reference genomes and genome annotations for *C. albicans* SC5314 (assembly 22), *C. glabrata* CBS138 and *C. parapsilosis* CDC317 were obtained from the *Candida* Genome Database (CGD, last accessed on 17 August 2017 (ref. <sup>91</sup>)). From the phased reference genome and annotations of *C. albicans*, we selected haplotype A to perform further analysis to avoid substantial rates of ambiguously mapped reads. The reference sequence and annotations for *C. tropicalis* were obtained from the RefSeq database (last accessed on 9 August 2017 (ref. <sup>92</sup>)). The genes missing from the RefSeq genome annotations were manually added from the *Candida* Gene Order Browser<sup>93</sup>. GFF genome annotation files were converted to GTF format using the gffread utility v.0.9.8 (ref. <sup>94</sup>). We used Centrifuge v.1.0.4 (ref. <sup>95</sup>) to test the presence of viral contamination in our dataset, by remapping the reads that mapped either to the human or fungal reference genomes to the whole National Center for Biotechnology Information nucleotide database (downloaded on 23 of March 2018). No traces of contamination were observed.

Differential gene expression analysis was performed using the Bioconductor package DESeq2 v.1.26.0 (ref. <sup>96</sup>) using the read counts obtained with STAR mapping. For human samples and each fungal species, we compared time point 0 with the other time points throughout the course of infection by Wald test using the contrast option of DESeq2. To detect any statistically significant changes of expression throughout the course of infection, we also used a likelihood ratio test of DESeq2, by dropping the 'time' component of the formula design. Genes with a log<sub>2</sub>(fold change) > 1.5 and adjusted  $P$  ( $P_{adj}$ ) < 0.01 were considered differentially expressed unless otherwise stated. To account for possible batch effects in the experiments involving *C. albicans* *ece1Δ/Δ* and non-viable fungal cells, we applied the RUVg function of the Bioconductor package RUVseq v.1.20 (ref. <sup>97</sup>) using non-differentially expressed genes (base mean > 10 and  $P_{adj}$  > 0.05 obtained by likelihood ratio test in DESeq2) across all samples and time points as negative controls. Since the optimal parameters for the batch effect removal algorithm are not defined a priori, we employed a strategy of incremental increase of  $k$  values ( $k=1, 2, \dots, n$ ), until we observed disruption of the PCA clustering of original data from the first batch of sequencing. To perform differential expression analysis, the obtained matrix of batch effect coefficients was further supplied to the design formula of the DESeq2 object, which was subsequently run using original count data. To plot 'batch-free' PCA plots, we used batch-corrected counts retrieved from the RUV package.

The list of 1-to-1 orthologues between the four fungal species was obtained from the CGD. For interspecies gene expression comparisons, the raw read counts for each fungal species were normalized by gene length and library size. GO term enrichment analysis was performed using clusterProfiler v.3.14.3 (ref. <sup>98</sup>). GO enrichment plots were produced with the dotplot function using showCategory set to 10 (for human data) and 8 (for fungal data) for better plot readability (the full list of GO enrichments is available in Supplementary File 9). Adjustment of  $P$  values was done using the Benjamini–Hochberg procedure. GO information for fungal species was obtained from the CGD, while for human data we used the Bioconductor package Genome wide annotation for Human (org.Hs.eg.db) v.3.10.0 in R<sup>99</sup>.

We assessed the patterns of host-pathogen gene coexpression across the infections using the weighted correlation network analysis approach implemented in WGCNA v.1.69 (ref. <sup>100</sup>). For each infection, we combined fungal and corresponding human data at all available time points of infection, excluding

the data for the *C. albicans* *ece1Δ/Δ* mutant. As recommended by the package developers, we selected genes that had 10 or more counts in more than 90% of samples for downstream analysis. As expression levels, we used variance-stabilized read count data obtained using the vst function of DESeq2. Before the actual network construction, we first selected the  $\beta$  power values using the pickSoftThreshold function implying an unsigned network. The minimum  $\beta$  values reaching 80% of scale-free network topology, namely 12, 20, 7 and 22 for infections with *C. albicans*, *C. glabrata*, *C. parapsilosis* and *C. tropicalis*, respectively, were used for downstream analysis. After network construction, we inferred modules (that is, highly interconnected clusters of genes) in the WGCNA networks using 1-topology overlap matrix values at the 0.25 hclust tree cut-off and identified eigengenes (that is, the first principal component of each module). For each identified module, we performed GO term enrichment analysis of fungal and host genes using clusterProfiler (Supplementary File 10), selecting the top 3 enrichments with the lowest  $P_{adj}$  values. Then, the fungal gene content of each module of a given fungal species was compared against those of all modules of the other three species taking into account 1-to-1 orthology information (Extended Data Fig. 3). This analysis was done for modules that contained at least one fungal gene. Similarity between fungal gene contents of two given modules was defined as the intersection of the fungal gene lists of these modules divided by the union of these gene lists.

All custom calculations and visualizations were performed in R v.3.6.1 using various packages (all packages and their versions are available at our GitHub page [https://github.com/Gabaldonlab/Host-pathogen\\_interactions](https://github.com/Gabaldonlab/Host-pathogen_interactions)).

**Statistics and reproducibility.** Experiments were performed in biological triplicates ( $n=3$ ) with 3 different donors (neutrophil cytokine release) or 3 independent experiments. The growth curve experiments (Fig. 1b) were performed five times to ensure reproducibility. Only the mitochondrial aspect ratio was calculated based on 1 biological replicate (Fig. 4d) but multiple mitochondria were measured for each condition ( $n > 80$ ). All microscopy findings were reliably reproduced. Data were analysed using Prism 8 (GraphPad Software). Values are presented as the mean  $\pm$  s.d. All the ratio data were log-transformed as indicated before statistical analysis in Prism and compared to 0 (uninfected/non-transfected/non-treated control) using a one-way analysis of variance (ANOVA) with Tukey's multiple comparisons test (Figs. 1b and 6b,d) or Dunnett's multiple comparisons test (Figs. 4e–g, 5c and 6a and Extended Data Fig. 5c,d), Kruskall–Wallis test with two-sided Dunn's multiple comparison test (Fig. 4d), two-tailed one-sample *t*-test (Fig. 5a) or two-way ANOVA and Sidak's multiple comparisons test (Fig. 5b,d). Statistical significance is indicated in the figures as \* $P \leq 0.05$ , \*\* $P \leq 0.01$ , \*\*\* $P \leq 0.001$  and \*\*\*\* $P \leq 0.0001$ . The exact *P* values are provided in the Source data.

**Reporting Summary.** Further information on research design is available in the Nature Research Reporting Summary linked to this article.

## Data availability

The data supporting the findings of this study are available within the paper and its Supplementary Information. All relevant data, including further image and processed data are available by request from the corresponding authors, with the restriction of data that would compromise the confidentiality of blood donors. Raw sequencing data have been deposited in the Sequence Read Archive under accession nos. SRR10279972–SRR10280067. Mapped data from the four *Candida* species can be mined and browsed at Candidamine (<http://candidamine.org/candidamine/begin.do>); the gene read counts from all samples can be found in our GitHub page [https://github.com/Gabaldonlab/Host-pathogen\\_interactions](https://github.com/Gabaldonlab/Host-pathogen_interactions) along with the data analysis scripts for results reproducibility. Publicly available datasets/databases used in the study can be accessed at: Ensembl (<https://www.ensembl.org/index.html>); RefSeq (<https://www.ncbi.nlm.nih.gov/refseq/>); CGOB (<http://cgob.ucd.ie/>); NCBI FTP site (<https://www.ncbi.nlm.nih.gov/home/download/>); CGD (<http://www.candidagenome.org/>); and Genome wide annotation for Human (<https://bioconductor.org/packages/release/data/annotation/html/org.Hs.eg.db.html>). Source data are provided with this paper.

## Code availability

All transcriptome data analysis results, including figures, extended data and supplementary materials are fully reproducible using the scripts provided at our GitHub page [https://github.com/Gabaldonlab/Host-pathogen\\_interactions](https://github.com/Gabaldonlab/Host-pathogen_interactions).

Received: 30 March 2020; Accepted: 1 February 2021;

Published online: 22 March 2021

## References

- Mårdh, P.-A. et al. Facts and myths on recurrent vulvovaginal candidosis: a review on epidemiology, clinical manifestations, diagnosis, pathogenesis and therapy. *Int. J. STD AIDS* **13**, 522–539 (2002).
- Fidel, P. L. Jr et al. An intravaginal live *Candida* challenge in humans leads to new hypotheses for the immunopathogenesis of vulvovaginal candidiasis. *Infect. Immun.* **72**, 2939–2946 (2004).
- Rosati, D., Bruno, M., Jaeger, M., Ten Oever, J. & Netea, M. G. Recurrent vulvovaginal candidiasis: an immunological perspective. *Microorganisms* **8**, 144 (2020).
- Yano, J. et al. Current patient perspectives of vulvovaginal candidiasis: incidence, symptoms, management and post-treatment outcomes. *BMC Womens Health* **19**, 48 (2019).
- Makanjuola, O., Bongomin, F. & Fayemiwo, S. A. An update on the roles of non-*albicans* *Candida* species in vulvovaginitis. *J. Fungi (Basel)* **4**, 121 (2018).
- Gabaldón, T., Naranjo-Ortíz, M. A. & Marcet-Houben, M. Evolutionary genomics of yeast pathogens in the Saccharomycotina. *FEMS Yeast Res.* **16**, fow064 (2016).
- Arastehfar, A. et al. Recent trends in molecular diagnostics of yeast infections: from PCR to NGS. *FEMS Microbiol. Rev.* **43**, 517–547 (2019).
- Meir, J. et al. Identification of *Candida albicans* regulatory genes governing mucosal infection. *Cell Microbiol.* **20**, e12841 (2018).
- Verma, A., Gaffen, S. L. & Swidergall, M. Innate immunity to mucosal *Candida* infections. *J. Fungi (Basel)* **3**, 60 (2017).
- Moreno-Ruiz, E. et al. *Candida albicans* internalization by host cells is mediated by a clathrin-dependent mechanism. *Cell Microbiol.* **11**, 1179–1189 (2009).
- Moyses, D. L. & Naglik, J. R. Mucosal immunity and *Candida albicans* infection. *Clin. Dev. Immunol.* **2011**, 346307 (2011).
- Moyses, D. L. et al. A biphasic innate immune MAPK response discriminates between the yeast and hyphal forms of *Candida albicans* in epithelial cells. *Cell Host Microbe* **8**, 225–235 (2010).
- Naglik, J. R. & Moyses, D. Epithelial cell innate response to *Candida albicans*. *Adv. Dent. Res.* **23**, 50–55 (2011).
- Naglik, J. R., Moyses, D. L., Wächtler, B. & Hube, B. *Candida albicans* interactions with epithelial cells and mucosal immunity. *Microbes Infect.* **13**, 963–976 (2011).
- Zhu, W. & Filler, S. G. Interactions of *Candida albicans* with epithelial cells. *Cell Microbiol.* **12**, 273–282 (2010).
- Westermann, A. J., Gorski, S. A. & Vogel, J. Dual RNA-seq of pathogen and host. *Nat. Rev. Microbiol.* **10**, 618–630 (2012).
- Hovhannisyan, H. & Gabaldón, T. Transcriptome sequencing approaches to elucidate host–microbe interactions in opportunistic human fungal pathogens. *Curr. Top. Microbiol. Immunol.* **422**, 193–235 (2019).
- Amorim-Vaz, S. et al. RNA enrichment method for quantitative transcriptional analysis of pathogens *in vivo* applied to the fungus *Candida albicans*. *mBio* **6**, e00942–15 (2015).
- Bruno, V. M. et al. Transcriptomic analysis of vulvovaginal candidiasis identifies a role for the NLRP3 inflammasome. *mBio* **6**, e00182–15 (2015).
- Liu, Y. et al. New signaling pathways govern the host response to *C. albicans* infection in various niches. *Genome Res.* **25**, 679–689 (2015).
- Tierney, L. et al. An interspecies regulatory network inferred from simultaneous RNA-seq of *Candida albicans* invading innate immune cells. *Front. Microbiol.* **3**, 85 (2012).
- Tóth, R. et al. Investigation of *Candida parapsilosis* virulence regulatory factors during host–pathogen interaction. *Sci. Rep.* **8**, 1346 (2018).
- Kämmer, P. et al. Survival strategies of pathogenic *Candida* species in human blood show independent and specific adaptations. *mBio* **11**, e02435–20 (2020).
- Huang, G. et al. Bistable expression of *WOR1*, a master regulator of white-opaque switching in *Candida albicans*. *Proc. Natl Acad. Sci. USA* **103**, 12813–12818 (2006).
- Richardson, J. P. et al. Candidalysin drives epithelial signaling, neutrophil recruitment, and immunopathology at the vaginal mucosa. *Infect. Immun.* **86**, e00645–17 (2018).
- Mills, E. L., Kelly, B. & O'Neill, L. A. J. Mitochondria are the powerhouses of immunity. *Nat. Immunol.* **18**, 488–498 (2017).
- Mohanty, A., Tiwari-Pandey, R. & Pandey, N. R. Mitochondria: the indispensable players in innate immunity and guardians of the inflammatory response. *J. Cell Commun. Signal.* **13**, 303–318 (2019).
- West, A. P. et al. Mitochondrial DNA stress primes the antiviral innate immune response. *Nature* **520**, 553–557 (2015).
- Pervolaraki, K. et al. Differential induction of interferon stimulated genes between type I and type III interferons is independent of interferon receptor abundance. *PLoS Pathog.* **14**, e1007420 (2018).
- Chen, Y., Zhou, Z. & Min, W. Mitochondria, oxidative stress and innate immunity. *Front. Physiol.* **9**, 1487 (2018).
- Zhang, Q. et al. Circulating mitochondrial DAMPs cause inflammatory responses to injury. *Nature* **464**, 104–107 (2010).
- Fridman, J. S. & Lowe, S. W. Control of apoptosis by p53. *Oncogene* **22**, 9030–9040 (2003).
- Schneider, W. M., Chevillotte, M. D. & Rice, C. M. Interferon-stimulated genes: a complex web of host defenses. *Annu. Rev. Immunol.* **32**, 513–545 (2014).

34. Smeekens, S. P. et al. Functional genomics identifies type I interferon pathway as central for host defense against *Candida albicans*. *Nat. Commun.* **4**, 1342 (2013).
35. El-Diwany, R. et al. CMPK2 and BCL-G are associated with type 1 interferon-induced HIV restriction in humans. *Sci. Adv.* **4**, eaat0843 (2018).
36. Sobel, J. D. et al. Vulvovaginal candidiasis: epidemiologic, diagnostic, and therapeutic considerations. *Am. J. Obstet. Gynecol.* **178**, 203–211 (1998).
37. Casadevall, A. & Pirofski, L.-A. The damage-response framework of microbial pathogenesis. *Nat. Rev. Microbiol.* **1**, 17–24 (2003).
38. Jabra-Rizk, M. A. et al. *Candida albicans* pathogenesis: fitting within the host-microbe damage response framework. *Infect. Immun.* **84**, 2724–2739 (2016).
39. Pirofski, L.-A. & Casadevall, A. The damage-response framework of microbial pathogenesis and infectious diseases. *Adv. Exp. Med. Biol.* **635**, 135–146 (2008).
40. Moyes, D. L. et al. Candidalysin is a fungal peptide toxin critical for mucosal infection. *Nature* **532**, 64–68 (2016).
41. Wilson, D., Naglik, J. R. & Hube, B. The missing link between *Candida albicans* hyphal morphogenesis and host cell damage. *PLoS Pathog.* **12**, e1005867 (2016).
42. Kearney, C. J., Randall, K. L. & Oliaro, J. DOCK8 regulates signal transduction events to control immunity. *Cell. Mol. Immunol.* **14**, 406–411 (2017).
43. Chu, E. Y. et al. Cutaneous manifestations of DOCK8 deficiency syndrome. *Arch. Dermatol.* **148**, 79–84 (2012).
44. McGhee, S. A. et al. DOCK8 deletions and mutations are associated with the autosomal recessive hyper-IgE phenotype. *J. Allergy Clin. Immunol.* **125**, AB356 (2010).
45. Zhang, Q. et al. Combined immunodeficiency associated with DOCK8 mutations. *N. Engl. J. Med.* **361**, 2046–2055 (2009).
46. Isaacs, A. & Lindenmann, J. Virus interference. I. The interferon. *Proc. R. Soc. Lond. B Biol. Sci.* **147**, 258–267 (1957).
47. Riedelberger, M. et al. Type I interferon response dysregulates host iron homeostasis and enhances *Candida glabrata* infection. *Cell Host Microbe* **27**, 454–466.e8 (2020).
48. Jaeger, M. et al. The RIG-I-like helicase receptor MDA5 (IFIH1) is involved in the host defense against *Candida* infections. *Eur. J. Clin. Microbiol. Infect. Dis.* **34**, 963–974 (2015).
49. del Fresno, C. et al. Interferon- $\beta$  production via Dectin-1-Syk-IRF5 signaling in dendritic cells is crucial for immunity to *C. albicans*. *Immunity* **38**, 1176–1186 (2013).
50. Kotredes, K. P., Thomas, B. & Gamero, A. M. The protective role of type I interferons in the gastrointestinal tract. *Front. Immunol.* **8**, 410 (2017).
51. Munakata, K. et al. Importance of the interferon- $\alpha$  system in murine large intestine indicated by microarray analysis of commensal bacteria-induced immunological changes. *BMC Genomics* **9**, 192 (2008).
52. Sato, M. et al. Positive feedback regulation of type I IFN genes by the IFN-inducible transcription factor IRF-7. *FEBS Lett.* **441**, 106–110 (1998).
53. Pekmezovic, M., Mogavero, S., Naglik, J. R. & Hube, B. Host-pathogen interactions during female genital tract infections. *Trends Microbiol.* **27**, 982–996 (2019).
54. Li, T., Liu, Z., Zhang, X., Chen, X. & Wang, S. Therapeutic effectiveness of type I interferon in vulvovaginal candidiasis. *Microp. Pathog.* **134**, 103562 (2019).
55. Lírio, J. et al. Antifungal (oral and vaginal) therapy for recurrent vulvovaginal candidiasis: a systematic review protocol. *BMJ Open* **9**, e027489 (2019).
56. Grazioli, S. & Pugin, J. Mitochondrial damage-associated molecular patterns: from inflammatory signaling to human diseases. *Front. Immunol.* **9**, 832 (2018).
57. Seth, R. B., Sun, L., Ea, C.-K. & Chen, Z. J. Identification and characterization of MAVS, a mitochondrial antiviral signaling protein that activates NF- $\kappa$ B and IRF 3. *Cell* **122**, 669–682 (2005).
58. West, A. P. & Shadel, G. S. Mitochondrial DNA in innate immune responses and inflammatory pathology. *Nat. Rev. Immunol.* **17**, 363–375 (2017).
59. Brokatzky, D. et al. A non-death function of the mitochondrial apoptosis apparatus in immunity. *EMBO J.* **38**, e100907 (2019).
60. Fang, C., Wei, X. & Wei, Y. Mitochondrial DNA in the regulation of innate immune responses. *Protein Cell* **7**, 11–16 (2016).
61. Kim, E. S. et al. Mitochondrial dynamics regulate melanogenesis through proteasomal degradation of MITF via ROS-ERK activation. *Pigment Cell Melanoma Res.* **27**, 1051–1062 (2014).
62. Plataki, M. et al. Mitochondrial dysfunction in aged macrophages and lung during primary *Streptococcus pneumoniae* infection is improved with pirfenidone. *Sci. Rep.* **9**, 971 (2019).
63. Ramond, E., Jamet, A., Coureuil, M. & Charbit, A. Pivotal role of mitochondria in macrophage response to bacterial pathogens. *Front. Immunol.* **10**, 2461 (2019).
64. West, A. P., Shadel, G. S. & Ghosh, S. Mitochondria in innate immune responses. *Nat. Rev. Immunol.* **11**, 389–402 (2011).
65. Kurihara, Y. et al. *Chlamydia trachomatis* targets mitochondrial dynamics to promote intracellular survival and proliferation. *Cell. Microbiol.* **21**, e12962 (2019).
66. Käding, N. et al. Growth of *Chlamydia pneumoniae* is enhanced in cells with impaired mitochondrial function. *Front. Cell. Infect. Microbiol.* **7**, 499 (2017).
67. Stavru, F., Bouillaud, F., Sartori, A., Ricquier, D. & Cossart, P. *Listeria monocytogenes* transiently alters mitochondrial dynamics during infection. *Proc. Natl. Acad. Sci. USA* **108**, 3612–3617 (2011).
68. Syn, G., Anderson, D., Blackwell, J. M. & Jamieson, S. E. *Toxoplasma gondii* infection is associated with mitochondrial dysfunction in-vitro. *Front. Cell. Infect. Microbiol.* **7**, 512 (2017).
69. Gao, Y. et al. Mitochondrial DNA leakage caused by *Streptococcus pneumoniae* hydrogen peroxide promotes type I IFN expression in lung cells. *Front. Microbiol.* **10**, 630 (2019).
70. Wang, P.-H. et al. A novel transcript isoform of STING that sequesters cGAMP and dominantly inhibits innate nucleic acid sensing. *Nucleic Acids Res.* **46**, 4054–4071 (2018).
71. Ning, X. et al. Apoptotic caspases suppress type I interferon production via the cleavage of cGAS, MAVS, and IRF3. *Mol. Cell* **74**, 19–31 (2019).
72. Ichim, G. et al. Limited mitochondrial permeabilization causes DNA damage and genomic instability in the absence of cell death. *Mol. Cell* **57**, 860–872 (2015).
73. Gillum, A. M., Tsay, E. Y. & Kirsch, D. R. Isolation of the *Candida albicans* gene for orotidine-5'-phosphate decarboxylase by complementation of *S. cerevisiae ura3* and *E. coli pyrF* mutations. *Mol. Gen. Genet.* **198**, 179–182 (1984).
74. Tavanti, A., Davidson, A. D., Gow, N. A., Maiden, M. C. & Odds, F. C. *Candida orthopsis* and *Candida metapsilosis* spp. nov. to replace *Candida parapsilosis* groups II and III. *J. Clin. Microbiol.* **43**, 284–292 (2005).
75. Hernandez, R. & Rupp, S. Human epithelial model systems for the study of *Candida* infections in vitro: part II. Histologic methods for studying fungal invasion. *Methods Mol. Biol.* **470**, 105–123 (2009).
76. Schaller, M., Zakikhany, K., Naglik, J. R., Weindl, G. & Hube, B. Models of oral and vaginal candidiasis based on *in vitro* reconstituted human epithelia. *Nat. Protoc.* **1**, 2767–2773 (2006).
77. Wächtler, B., Wilson, D., Haedicke, K., Dalle, F. & Hube, B. From attachment to damage: defined genes of *Candida albicans* mediate adhesion, invasion and damage during interaction with oral epithelial cells. *PLoS ONE* **6**, e17046 (2011).
78. Liu, Y., Zhou, J. & White, K. P. RNA-seq differential expression studies: more sequence or more replication? *Bioinformatics* **30**, 301–304 (2014).
79. Hovhannisyan, H., Hafez, A., Llorens, C. & Gabaldón, T. CROSSMAPPER: estimating cross-mapping rates and optimizing experimental design in multi-species sequencing studies. *Bioinformatics* **36**, 925–927 (2020).
80. Chan, F. K., Moriwaki, K. & De Rosa, M. J. Detection of necrosis by release of lactate dehydrogenase activity. *Methods Mol. Biol.* **979**, 65–70 (2013).
81. Bronner, D. N. & O'Riordan, M. X. Measurement of mitochondrial DNA release in response to ER stress. *Bio Protoc.* **6**, e1839 (2016).
82. Win, S., Than, T. A., Fernandez-Checa, J. C. & Kaplowitz, N. JNK interaction with Sab mediates ER stress induced inhibition of mitochondrial respiration and cell death. *Cell Death Dis.* **5**, e989 (2014).
83. Bannwarth, S., Procaccio, V. & Paquis-Flucklinger, V. Rapid identification of unknown heteroplasmic mutations across the entire human mitochondrial genome with mismatch-specific Surveyor Nuclease. *Nat. Protoc.* **1**, 2037–2047 (2006).
84. Gresnigt, M. S. et al. Neutrophil-mediated inhibition of proinflammatory cytokine responses. *J. Immunol.* **189**, 4806–4815 (2012).
85. Picard, M., White, K. & Turnbull, D. M. Mitochondrial morphology, topology, and membrane interactions in skeletal muscle: a quantitative three-dimensional electron microscopy study. *J. Appl. Physiol.* **114**, 161–171 (2013).
86. Andrews, S. *FastQC: a Quality Control Tool for High Throughput Sequence Data* <http://www.bioinformatics.babraham.ac.uk/projects/fastqc> (2010).
87. Ewels, P., Magnusson, M., Lundin, S. & Käller, M. MultiQC: summarize analysis results for multiple tools and samples in a single report. *Bioinformatics* **32**, 3047–3048 (2016).
88. Bolger, A. M., Lohse, M. & Usadel, B. Trimmomatic: a flexible trimmer for Illumina sequence data. *Bioinformatics* **30**, 2114–2120 (2014).
89. Dobin, A. et al. STAR: ultrafast universal RNA-seq aligner. *Bioinformatics* **29**, 15–21 (2013).
90. Hunt, S. E. et al. Ensembl variation resources. *Database (Oxford)* **2018**, bay119 (2018).
91. Skrzypek, M. S. et al. The *Candida* Genome Database (CGD): incorporation of Assembly 22, systematic identifiers and visualization of high throughput sequencing data. *Nucleic Acids Res.* **45**, D592–D596 (2017).

92. O'Leary, N. A. et al. Reference sequence (RefSeq) database at NCBI: current status, taxonomic expansion, and functional annotation. *Nucleic Acids Res.* **44**, D733–D745 (2016).
93. Maguire, S. L. et al. Comparative genome analysis and gene finding in *Candida* species using CGOB. *Mol. Biol. Evol.* **30**, 1281–1291 (2013).
94. Trapnell, C. et al. Transcript assembly and quantification by RNA-Seq reveals unannotated transcripts and isoform switching during cell differentiation. *Nat. Biotechnol.* **28**, 511–515 (2010).
95. Kim, D., Song, L., Breitwieser, F. P. & Salzberg, S. L. Centrifuge: rapid and sensitive classification of metagenomic sequences. *Genome Res.* **26**, 1721–1729 (2016).
96. Love, M. I., Huber, W. & Anders, S. Moderated estimation of fold change and dispersion for RNA-seq data with DESeq2. *Genome Biol.* **15**, 550 (2014).
97. Risso, D., Ngai, J., Speed, T. P. & Dudoit, S. Normalization of RNA-seq data using factor analysis of control genes or samples. *Nat. Biotechnol.* **32**, 896–902 (2014).
98. Yu, G., Wang, L.-G., Han, Y. & He, Q.-Y. clusterProfiler: an R package for comparing biological themes among gene clusters. *OMICS* **16**, 284–287 (2012).
99. Carlson, M. *org.Hs.eg.db: Genome wide annotation for Human*. R package version 3.10.0 <https://www.bioconductor.org/packages/release/data/annotation/html/org.Hs.eg.db.html> (2019).
100. Langfelder, P. & Horvath, S. WGCNA: an R package for weighted correlation network analysis. *BMC Bioinformatics* **9**, 559 (2008).

## Acknowledgements

M.P., H.H., E.I., J.O.P., T.G., G.B. and B.H. received funding from the European Union Horizon 2020 research and innovation programme under the Marie Skłodowska-Curie grant no. 642095 (OPATHY). B.H. also received support from the German Research Foundation within the Collaborative Research Centre/Transregio 124 FungiNet (project C1). M.S.G. was supported by the German Research Foundation Emmy Noether Programme (project no. 434385622/GR 5617/1-1). We acknowledge the support of the Spanish Ministry of Science, Innovation and Universities (grant no. PGC2018-099921-B-I00) to the European Molecular Biology Laboratory partnership, the Centro de Excelencia Severo Ochoa and the CERCA Programme/Generalitat de Catalunya.

We thank C. Kämnnitz from the Electron Microscopy Center in Jena for the sample preparation for TEM. The schematic models in Figs. 4–6 were created with images adapted from Servier Medical Art (Servier).

## Author contributions

M.P. performed all the laboratory experiments (except for TEM), analysed the data, wrote the manuscript and prepared the figures. H.H. performed all the bioinformatics analyses, wrote the manuscript and prepared the figures. E.I. and J.O.P. performed the infection experiments for RNA-seq and edited the manuscript. S.S.L. performed the growth curve and flow cytometry experiments and helped with the mtDNA depletion set-up, including the data analysis. T. Kalkreuter performed additional RT-qPCR experiments. S. Müller and T. Kamradt contributed to the additional mitochondrial phenotypic assays and data interpretation. E.S. and B.Q. performed the TEM experiments, analysed the data and edited the manuscript. M.S.G., S. Mogavero, S.B. and G.B. designed the experiments and edited the manuscript. B.H. and T.G. conceived and designed the study and wrote the manuscript.

## Competing interests

The authors declare no competing interests.

## Additional information

**Extended data** is available for this paper at <https://doi.org/10.1038/s41564-021-00875-2>.

**Supplementary information** The online version contains supplementary material available at <https://doi.org/10.1038/s41564-021-00875-2>.

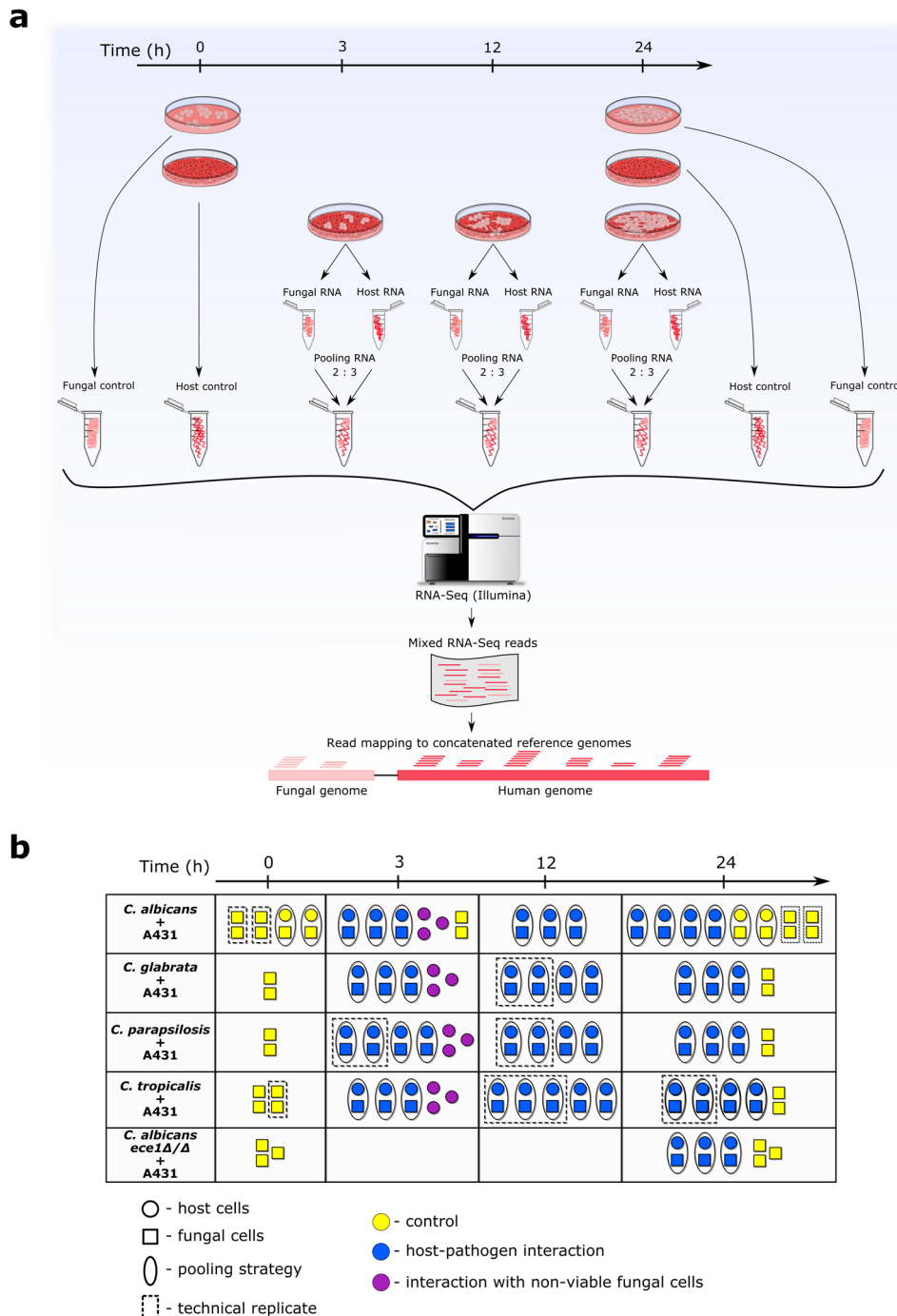
**Correspondence and requests for materials** should be addressed to T.G. or B.H.

**Peer review information** *Nature Microbiology* thanks Elaine Bignell, Robert Watson and the other, anonymous, reviewer(s) for their contribution to the peer review of this work. Peer reviewer reports are available.

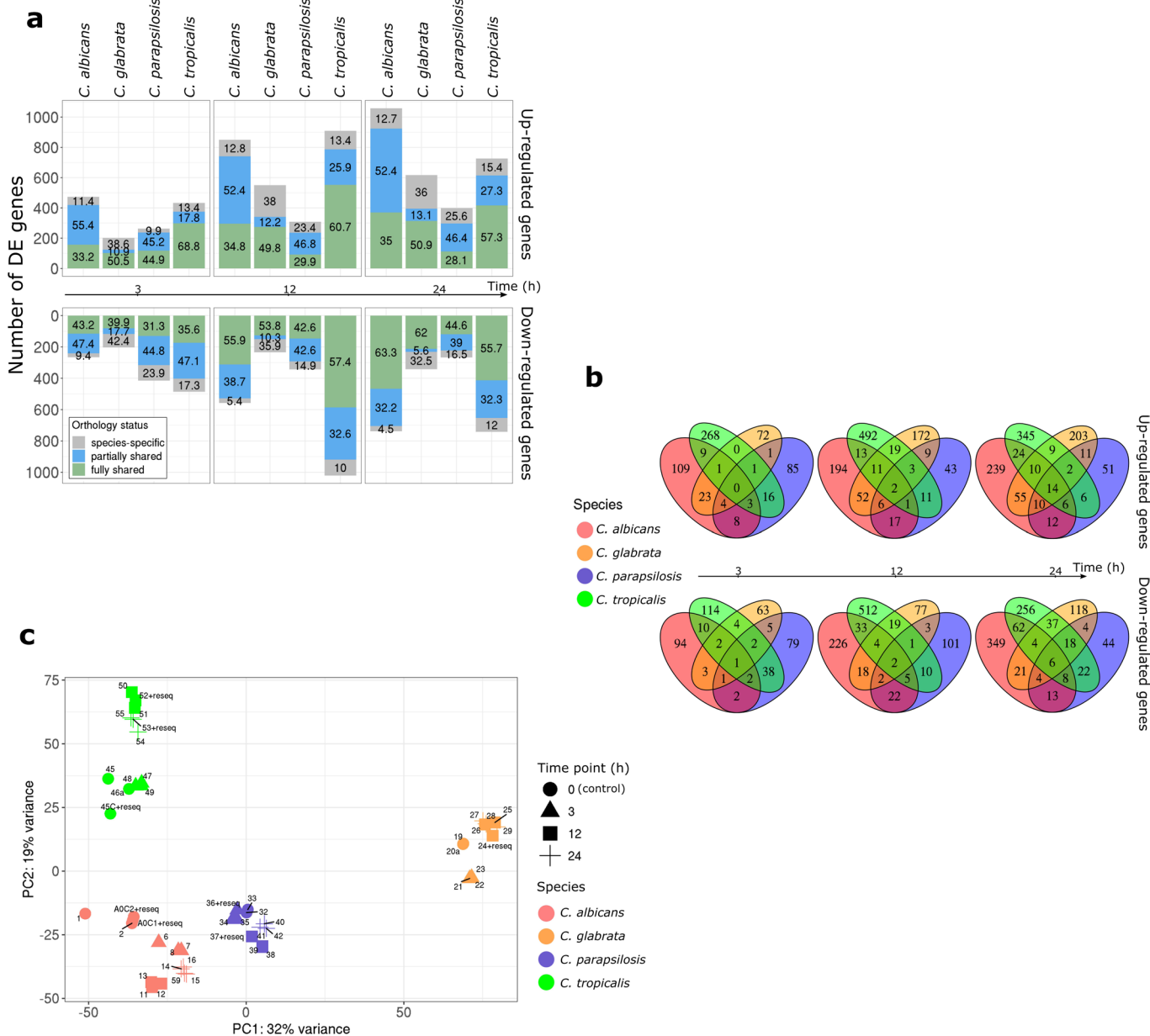
**Reprints and permissions information** is available at [www.nature.com/reprints](http://www.nature.com/reprints).

**Publisher's note** Springer Nature remains neutral with regard to jurisdictional claims in published maps and institutional affiliations.

© The Author(s), under exclusive licence to Springer Nature Limited 2021

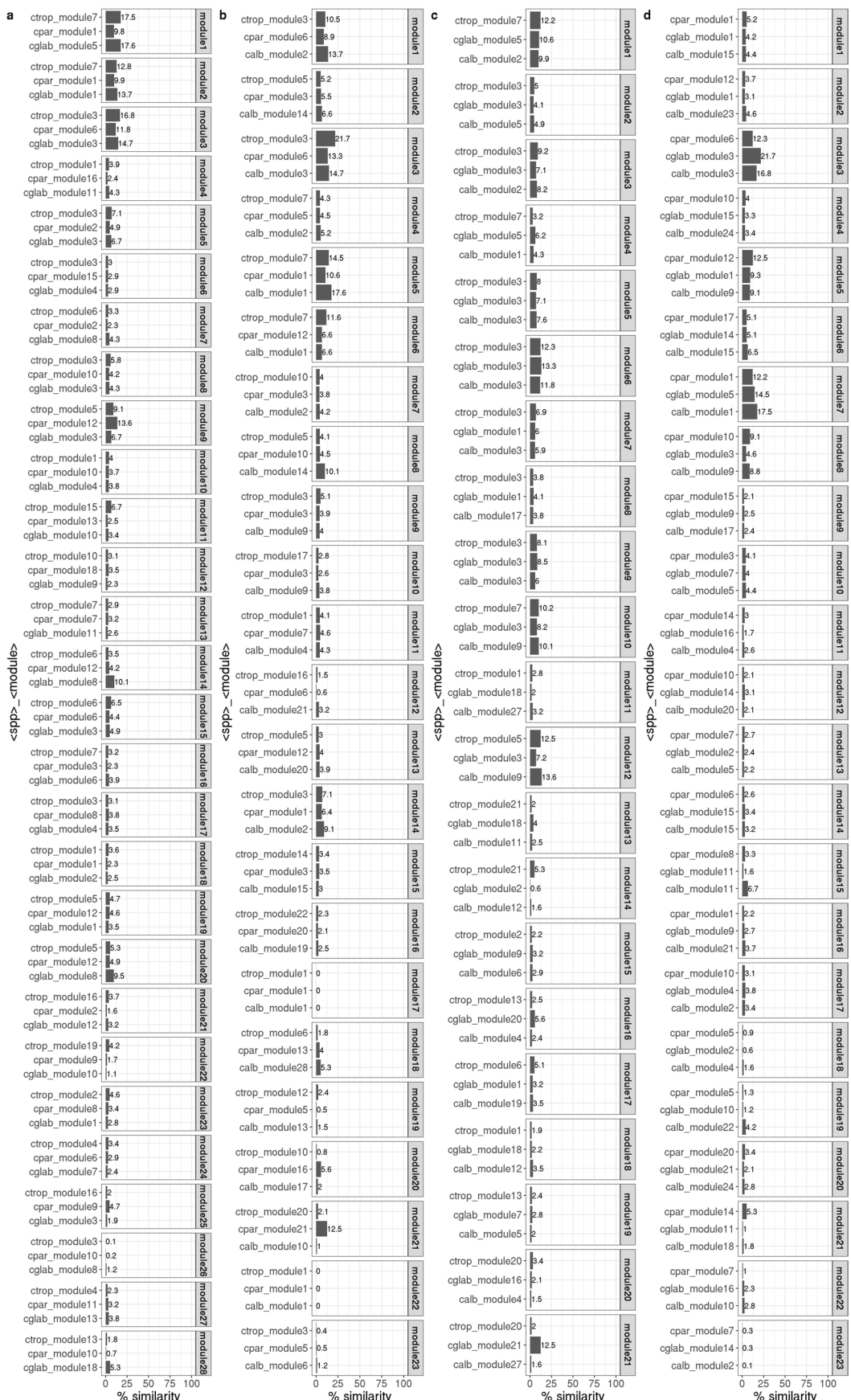


**Extended Data Fig. 1 | Overall experimental design of the current study.** **a**, Schematic representation of the experimental design. Each *Candida* species was co-cultivated with host cells. Controls included samples at 0 and 24 h for both host and yeasts alone. At the indicated time points of infection, fungal and host RNAs were independently extracted and subsequently combined (pooled) at a 2:3 fungus-to-host ratio into one sample for library preparation and sequencing. Sequencing data were mapped to a concatenated host and fungal reference genome. **b**, Schematic representation of the entire study including all samples. Each symbol corresponds to a sequenced sample (or technical replicates of the same sample). Host samples are depicted with circles; *Candida* samples are depicted with squares; the strategy for combining (pooling) human and fungal RNAs in the same sequencing library is shown with ovals surrounding the corresponding samples; technical replicates (that is the same sequencing library sequenced several times) are surrounded with dashed rectangles. Control samples are depicted in yellow; interacting host and fungal samples are depicted in blue; host samples interacting with non-viable fungal cells are depicted in purple. Each row indicates the samples for each human-yeast interaction experiment.



#### Extended Data Fig. 2 | Distinct patterns of transcriptome profiles of the four *Candida* species upon interaction with human epithelial cells. a,

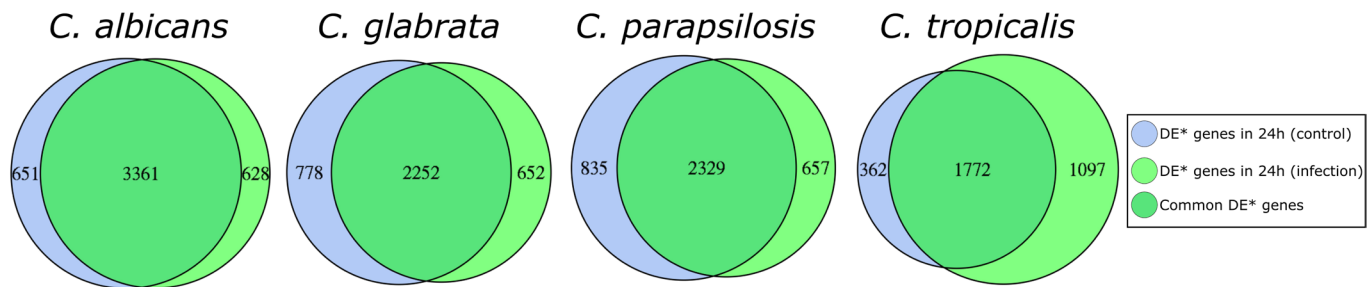
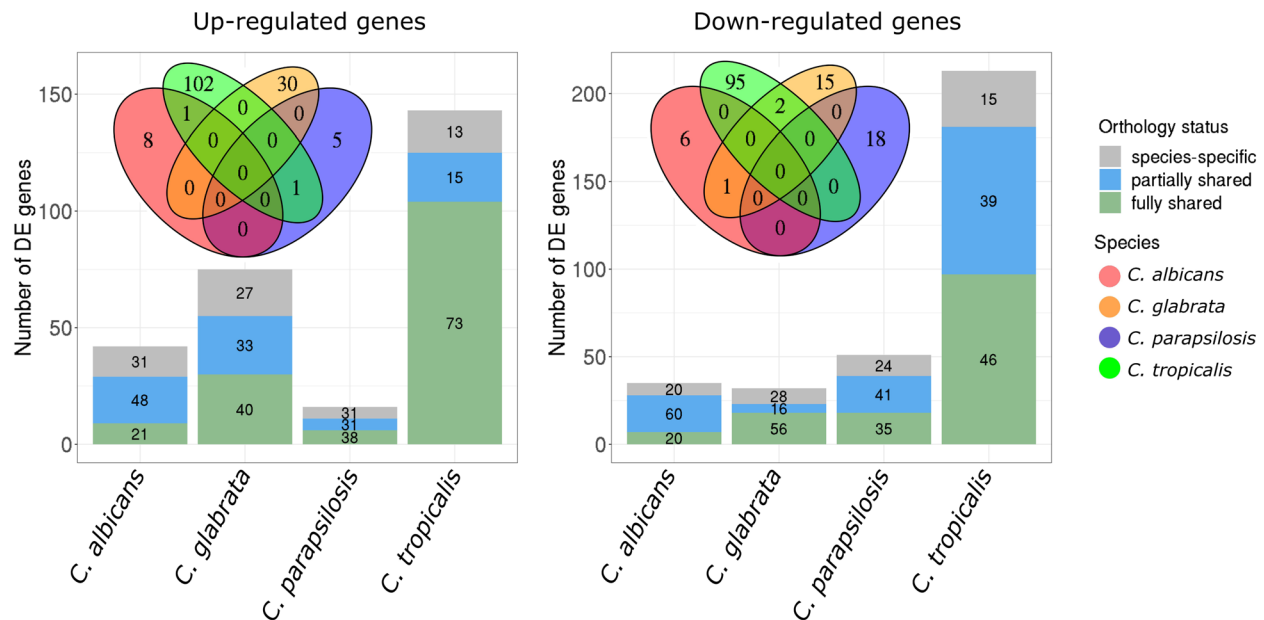
Distribution of fully shared, partially shared and species-specific differentially expressed (DE) genes across the course of infections. Numbers on bar plots indicate the percentage (%). b, Venn diagrams of DE genes (only 1-to-1 orthologs) in four *Candida* species at each time point. c, PCA biplot based on expression levels of orthologous genes across *Candida* species, demonstrating a species-specific stratification of transcriptomic profiles of the four fungal pathogens; Labels of the data points correspond to sample identifiers, where 'reseq' indicates that the sample was sequenced more than once (see Supplementary Table 1 for details).



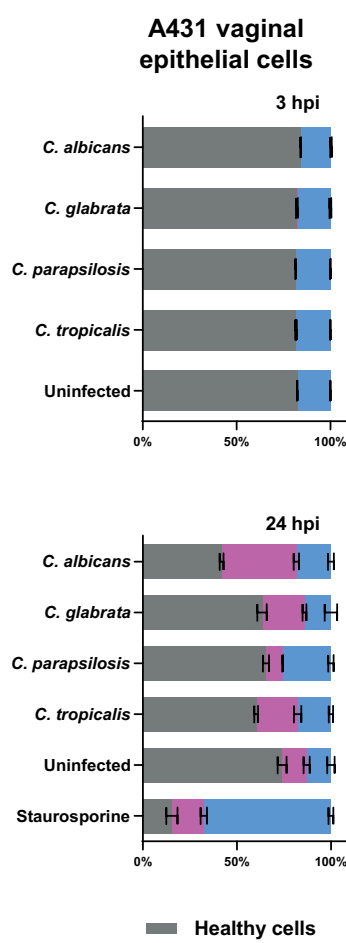
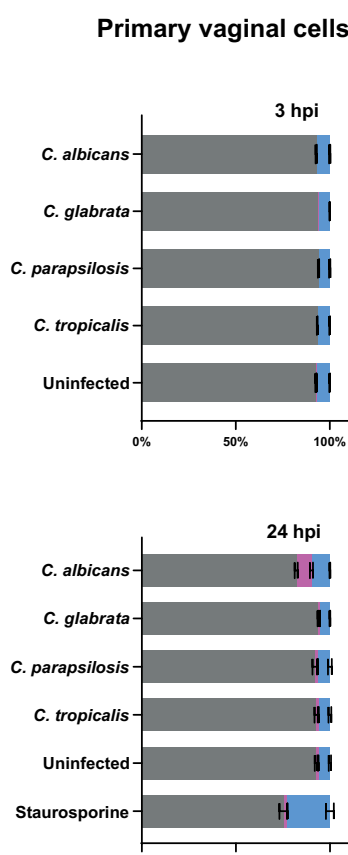
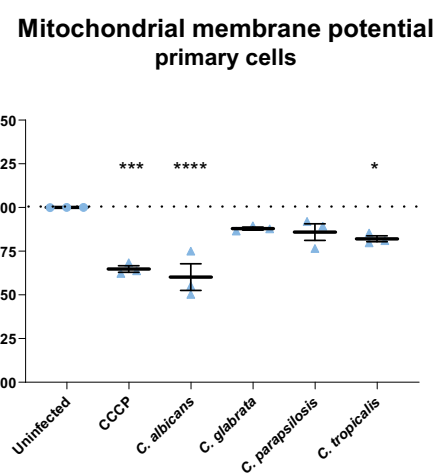
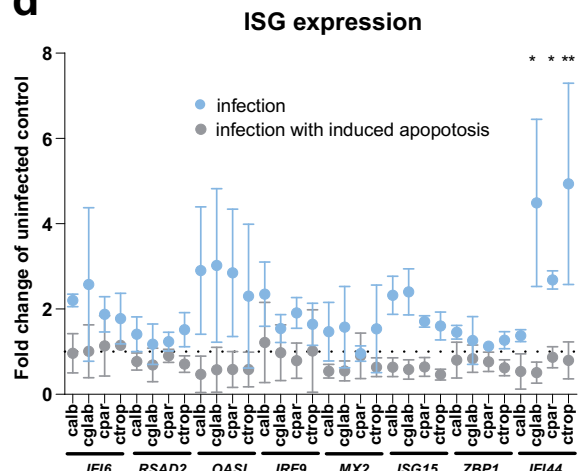
Extended Data Fig. 3 | See next page for caption.

**Extended Data Fig. 3 | Comparison of orthologous gene content similarities between co-expressed gene modules in different yeast species. a,**

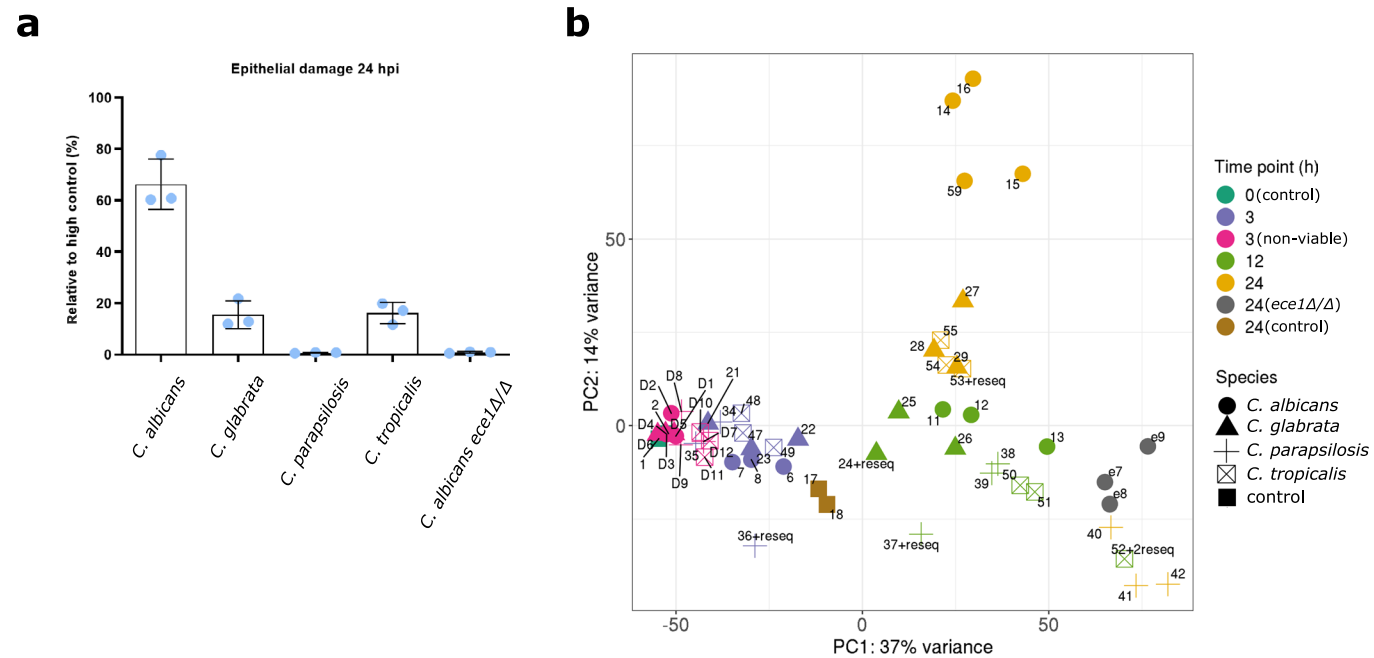
Comparison of *C. albicans* modules against modules of other species. **b**, Comparison of *C. glabrata* modules against modules of other species. **c**, Comparison of *C. parapsilosis* modules against modules of other species. **d**, Comparison of *C. tropicalis* modules against modules of other species. Each box represents a module of a given species (reference module); the title of a box represents the reference module name. Each reference module is compared with all modules of other three species, and the modules of other species with the highest similarity to the reference module are plotted with horizontal bars, representing level of similarity (in %). Labels of the horizontal bars indicate <species name>\_<module name>. 'calb' denotes *C. albicans*, 'cglab' - *C. glabrata*, 'cpar' - *C. parapsilosis*, 'ctrop' - *C. tropicalis*. The level of similarity refers to the fraction (in %) of shared one-to-one orthologous genes between two given modules, defined as the intersection of gene lists of orthologs of two modules divided by the union of these gene lists.

**a****b**

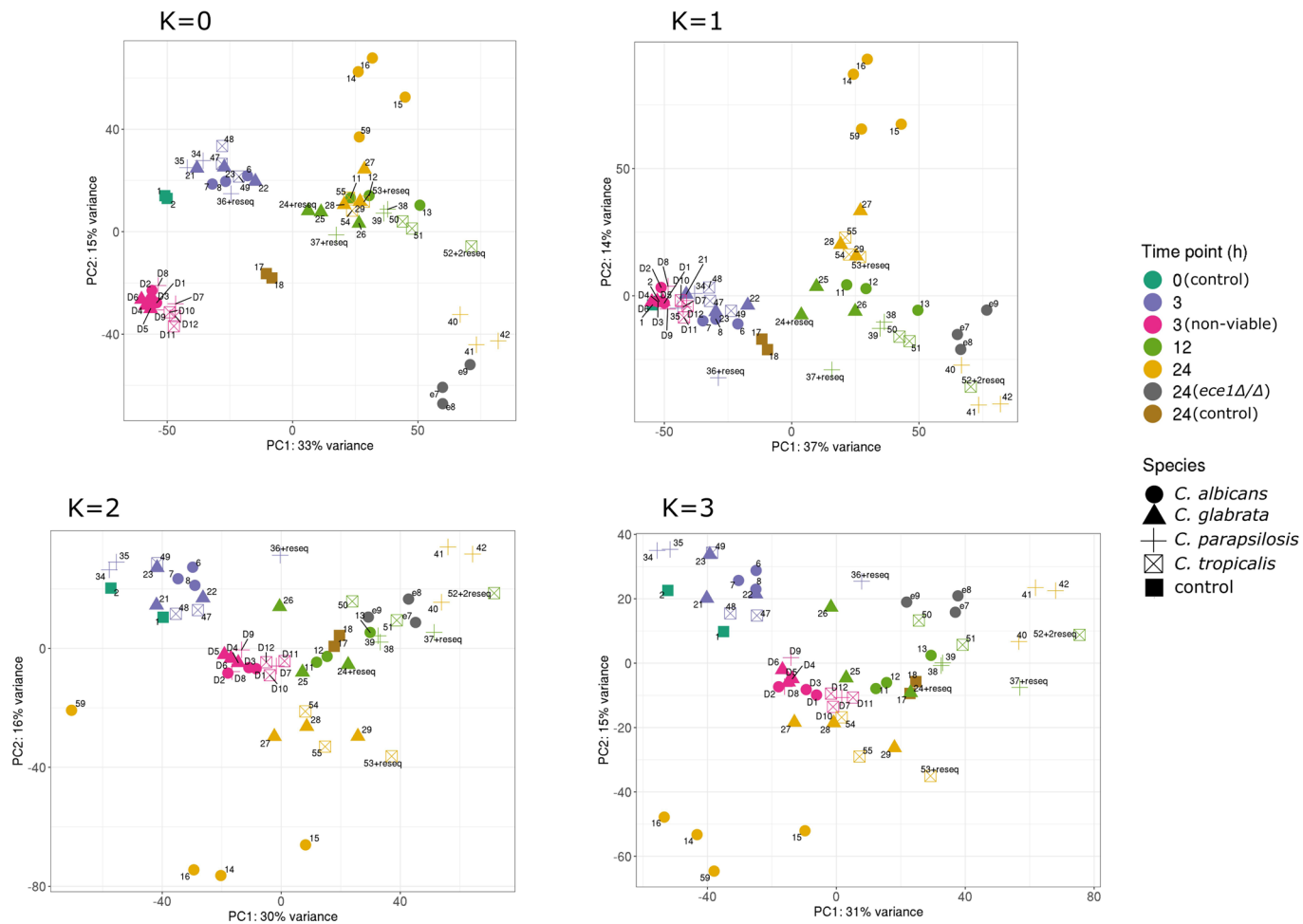
**Extended Data Fig. 4 | Infection-specific differentially expressed (DE) genes of Candida species.** **a**, Venn diagrams indicating similarities and differences of fungal DE\* genes in culture medium only (control) and in response to epithelial cells (infection). \*To identify infection-specific genes with a higher stringency, we applied filters of  $|\log_2 \text{fold change}| > 0$  and  $p_{\text{adj}} < 0.01$ . For the downstream analysis of identified genes, we used a filtering of  $|\log_2 \text{fold change}| > 1.5$  and  $p_{\text{adj}} < 0.01$  for consistency with other results. Differential expression analysis was done using DESeq2 v. 1.26.0 and comparisons against time point 0 were done using the two-sided Wald test. **b**, Distribution of infection-specific fungal genes across the studied *Candida* pathogens. Bar plots demonstrate the distribution of partially shared, fully shared, and species-specific genes. Numbers on bar plots indicate the percentage (%). Venn diagrams depict numbers of fully shared genes (1-to-1 orthologs) across species.

**a****b****c****d**

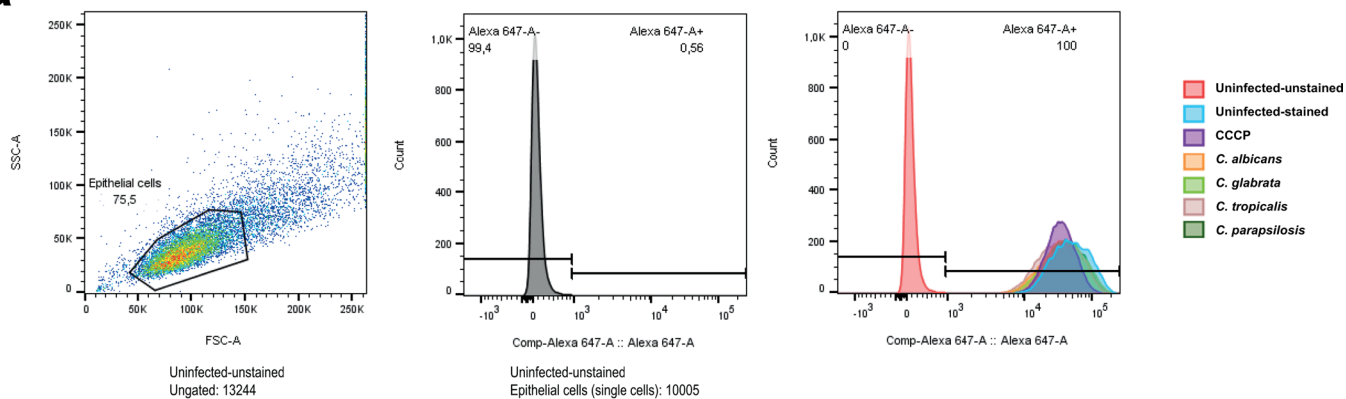
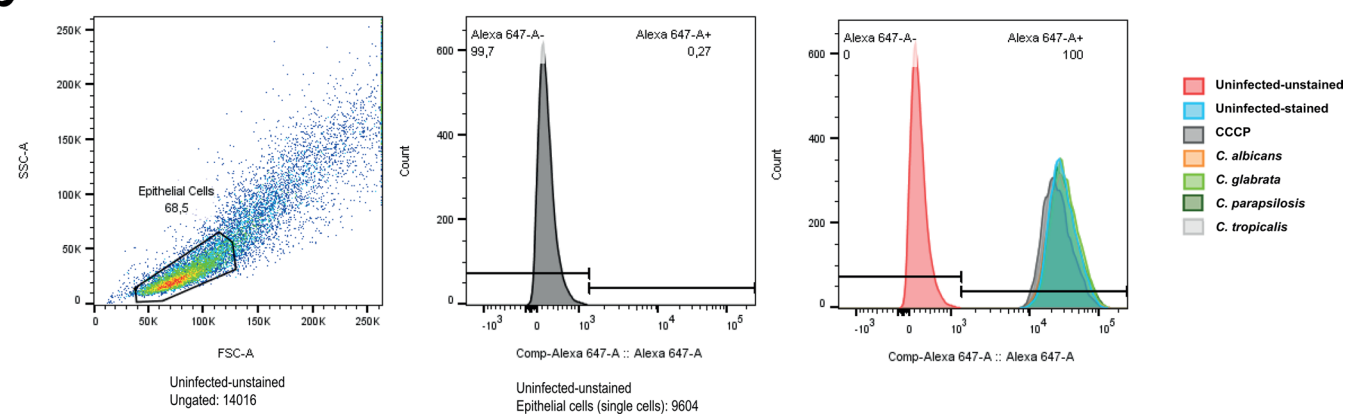
**Extended Data Fig. 5 | Candida species induce type I interferon signalling independently of apoptosis.** The proportion of healthy, necrotic, and apoptotic vaginal epithelial cells (ECs) 3 and 24 hours post-infection (hpi) with *Candida* in (a) A431 vaginal ECs used throughout this study and (b) primary vaginal ECs. Treatment with 1.2 µM staurosporine was used as a positive control. (c) Mitochondrial membrane potential change of primary vaginal ECs at 1 hpi, positive control CCCP 100 µM. (d) Relative expression (RT-qPCR) of selected Interferon-Stimulated Genes (ISGs) in *C. albicans*-infected ECs where apoptosis was induced with 1.2 µM staurosporine at 3 hpi. All values are presented as mean ± SD of n=3 independent experiments. Statistical significance is indicated as: \*, p ≤ 0.05; \*\*\*, p ≤ 0.001; \*\*, p ≤ 0.0001 (one-way ANOVA with Dunnett's multiple comparisons test (c-d); 'calb' denotes *C. albicans*, 'cglab' - *C. glabrata*, 'cpar' - *C. parapsilosis*, 'ctrop' - *C. tropicalis*.



**Extended Data Fig. 6 | Human transcriptome profiles response to fungal damage.** **a**, Levels of LDH release by epithelial cells upon the damage by four fungal pathogens 24 hpi. All values are presented as mean  $\pm$  SD of  $n=3$  independent experiments. **b**, PCA plot of human samples interacting with non-viable and viable fungal species, including *C. albicans ece1Δ/Δ*. The plot is obtained using the RUVg function of RUVseq with  $k=1$  (see Extended Data Fig. 7 for plots with alternative  $k$  values). Labels of the data points correspond to sample identifiers, where 'reseq' indicates that the sample was sequenced more than once (see Supplementary Table 1 for details). 'non-viable' indicates host samples interacting with non-viable fungal cells; '*ece1Δ/Δ*' indicates host samples interacting with *C. albicans ece1Δ/Δ*.



**Extended Data Fig. 7 | Human transcriptome response assessed with different parameters of batch effect correction.** PCA plots of human samples interacting with fungal cells obtained using  $k=0, 1, 2, 3$  values of RUVseq package for batch effect correction. Labels of the data points correspond to sample identifiers, where 'reseq' indicates that the sample was sequenced more than once (see Supplementary Table 1 for details). 'non-viable' indicates host samples interacting with non-viable fungal cells; ' $ece1\Delta/\Delta$ ' indicates host samples interacting with *C. albicans*  $ece1\Delta/\Delta$ .

**a****b**

**Extended Data Fig. 8 | Applied gating strategies across flow cytometry experiments for epithelial cells.** **a**, A431 cells (linked to Fig. 4e) and **(b)** primary vaginal cells (linked to Extended Data Fig. 6c). First,  $10^4$  events were analyzed based on their side scatter area (SSC-A) vs. forward scatter area (FSC-A). For further analysis, single cells were selected based on forward scatter height (FSC-H) vs. forward scatter area (FSC-A). MitoTracker® Deep Red FM signal was measured using detection channel Alexa 647-A. The unstained population was taken as a reference to determine the median fluorescence intensity of all samples (depicted as histogram Alexa 647-A- and Alexa 647-A+). The ratio from the median intensity of the stained/uninfected cells and unstained/uninfected cells was used as a reference to obtain the results of the infected samples shown in the manuscript figures.

## Reporting Summary

Nature Research wishes to improve the reproducibility of the work that we publish. This form provides structure for consistency and transparency in reporting. For further information on Nature Research policies, see [Authors & Referees](#) and the [Editorial Policy Checklist](#).

### Statistical parameters

When statistical analyses are reported, confirm that the following items are present in the relevant location (e.g. figure legend, table legend, main text, or Methods section).

n/a Confirmed

- The exact sample size ( $n$ ) for each experimental group/condition, given as a discrete number and unit of measurement
- An indication of whether measurements were taken from distinct samples or whether the same sample was measured repeatedly
- The statistical test(s) used AND whether they are one- or two-sided  
*Only common tests should be described solely by name; describe more complex techniques in the Methods section.*
- A description of all covariates tested
- A description of any assumptions or corrections, such as tests of normality and adjustment for multiple comparisons
- A full description of the statistics including central tendency (e.g. means) or other basic estimates (e.g. regression coefficient) AND variation (e.g. standard deviation) or associated estimates of uncertainty (e.g. confidence intervals)
- For null hypothesis testing, the test statistic (e.g.  $F$ ,  $t$ ,  $r$ ) with confidence intervals, effect sizes, degrees of freedom and  $P$  value noted  
*Give P values as exact values whenever suitable.*
- For Bayesian analysis, information on the choice of priors and Markov chain Monte Carlo settings
- For hierarchical and complex designs, identification of the appropriate level for tests and full reporting of outcomes
- Estimates of effect sizes (e.g. Cohen's  $d$ , Pearson's  $r$ ), indicating how they were calculated
- Clearly defined error bars  
*State explicitly what error bars represent (e.g. SD, SE, CI)*

*Our web collection on [statistics for biologists](#) may be useful.*

### Software and code

Policy information about [availability of computer code](#)

Data collection

Microsoft Excel 2010, BD FACSuite v1.0.6.5230, Bio-Rad CFX Manager 3.1, FC, ZEN 2.6 Blue Edition

Data analysis

FlowJO™ 10.2 , GraphPad Prism 8, ImageJ version 1.43h, ZEN 2.6 Blue Edition, FastQC v.0.11.6, Multiqc v.1.0, Trimmomatic v.0.36, STAR v.2.5.2b, gffread v.0.9.8, Centrifuge v.1.0.4, Crossmapper v.1.1.0, DESeq2 v.1.26.0, RUVseq v.1.20, clusterProfiler v.3.14.3, org.Hs.eg.db v.3.10.0, WGCNA v.1.69, R v.3.6.1 using various packages (available at our GitHub page [https://github.com/Gabaldonlab/Host-pathogen\\_interactions](https://github.com/Gabaldonlab/Host-pathogen_interactions)).

For manuscripts utilizing custom algorithms or software that are central to the research but not yet described in published literature, software must be made available to editors/reviewers upon request. We strongly encourage code deposition in a community repository (e.g. GitHub). See the Nature Research [guidelines for submitting code & software](#) for further information.

## Data

Policy information about [availability of data](#)

All manuscripts must include a [data availability statement](#). This statement should provide the following information, where applicable:

- Accession codes, unique identifiers, or web links for publicly available datasets
- A list of figures that have associated raw data
- A description of any restrictions on data availability

The authors declare that the data supporting the findings of this study are available within the paper and its supporting files, including source data. All relevant data, including further image data and processed data are available by request from the corresponding authors, with the restriction of data that would compromise confidentiality of blood donors. Raw sequencing data have been deposited in SRA under the accession numbers SRR10279972-SRR10280067. Mapped data from the four Candida species can be mined and browsed at Candidamine ([candidamine.org](http://candidamine.org)) and gene read counts from all samples can be found in our GitHub page [https://github.com/Gabaldonlab/Host-pathogen\\_interactions](https://github.com/Gabaldonlab/Host-pathogen_interactions) along with data analysis scripts for results reproducibility. Publicly available datasets/databases used in the study are: Ensembl (<https://www.ensembl.org/index.html>, last accessed on 08/08/2017), RefSeq (<https://www.ncbi.nlm.nih.gov/refseq/>, last accessed on 09/08/2017), CGOB (<http://cgob.ucd.ie/>, last accessed on 09/08/2017), NCBI nt database (<https://www.ncbi.nlm.nih.gov/home/download/>, last accessed on 23/03/2018), Candida Genome Database (<http://www.candidagenome.org/>, last accessed on 17/08/2017), Genome-wide annotation for Human database (<https://bioconductor.org/packages/release/data/annotation/html/org.Hs.eg.db.html>, last accessed on 10/03/2020).

## Field-specific reporting

Please select the best fit for your research. If you are not sure, read the appropriate sections before making your selection.

Life sciences       Behavioural & social sciences       Ecological, evolutionary & environmental sciences

For a reference copy of the document with all sections, see [nature.com/authors/policies/ReportingSummary-flat.pdf](https://www.nature.com/authors/policies/ReportingSummary-flat.pdf)

## Life sciences study design

All studies must disclose on these points even when the disclosure is negative.

Sample size	No sample size calculations were performed. Most experiments were done in triplicates, which is a normally employed sample size to ensure biological reproducibility, unless otherwise stated. For growth curves (Fig. 1b), experiments were performed five times to better ensure the reproducibility. Only mitochondrial aspect ratio was calculated based on one biological replicate (Fig. 4d), but multiple mitochondria were measured for each condition ( $n>80$ ) to ensure the reliability of the results. Sample size of each experiment is stated in Materials and methods and Figure legends.
Data exclusions	No data was excluded.
Replication	All experiments were independently repeated at least three times, unless otherwise stated. All findings were reliably reproduced. Details for each experiment are provided in the Figure legends and Materials and methods.
Randomization	To avoid potential batch and lane effects during sequencing, all samples were randomly distributed on the sequencing flowcells. There were no other variables or interventions to randomize in this study.
Blinding	Blinding was applied only for the experiments where qualitative scoring was applied (microscopy, Fig. 4b-d) to avoid potential bias in image acquisition and analyses. For other experiments, blinding was either not possible or not relevant.

## Behavioural & social sciences study design

All studies must disclose on these points even when the disclosure is negative.

Study description	Briefly describe the study type including whether data are quantitative, qualitative, or mixed-methods (e.g. qualitative cross-sectional, quantitative experimental, mixed-methods case study).
Research sample	State the research sample (e.g. Harvard university undergraduates, villagers in rural India) and provide relevant demographic information (e.g. age, sex) and indicate whether the sample is representative. Provide a rationale for the study sample chosen. For studies involving existing datasets, please describe the dataset and source.
Sampling strategy	Describe the sampling procedure (e.g. random, snowball, stratified, convenience). Describe the statistical methods that were used to predetermine sample size OR if no sample-size calculation was performed, describe how sample sizes were chosen and provide a rationale for why these sample sizes are sufficient. For qualitative data, please indicate whether data saturation was considered, and what criteria were used to decide that no further sampling was needed.
Data collection	Provide details about the data collection procedure, including the instruments or devices used to record the data (e.g. pen and paper, computer, eye tracker, video or audio equipment) whether anyone was present besides the participant(s) and the researcher, and whether the researcher was blind to experimental condition and/or the study hypothesis during data collection.

Timing	Indicate the start and stop dates of data collection. If there is a gap between collection periods, state the dates for each sample cohort.
Data exclusions	If no data were excluded from the analyses, state so OR if data were excluded, provide the exact number of exclusions and the rationale behind them, indicating whether exclusion criteria were pre-established.
Non-participation	State how many participants dropped out/declined participation and the reason(s) given OR provide response rate OR state that no participants dropped out/declined participation.
Randomization	If participants were not allocated into experimental groups, state so OR describe how participants were allocated to groups, and if allocation was not random, describe how covariates were controlled.

## Ecological, evolutionary & environmental sciences study design

All studies must disclose on these points even when the disclosure is negative.

Study description	Briefly describe the study. For quantitative data include treatment factors and interactions, design structure (e.g. factorial, nested, hierarchical), nature and number of experimental units and replicates.
Research sample	Describe the research sample (e.g. a group of tagged <i>Passer domesticus</i> , all <i>Stenocereus thurberi</i> within Organ Pipe Cactus National Monument), and provide a rationale for the sample choice. When relevant, describe the organism taxa, source, sex, age range and any manipulations. State what population the sample is meant to represent when applicable. For studies involving existing datasets, describe the data and its source.
Sampling strategy	Note the sampling procedure. Describe the statistical methods that were used to predetermine sample size OR if no sample-size calculation was performed, describe how sample sizes were chosen and provide a rationale for why these sample sizes are sufficient.
Data collection	Describe the data collection procedure, including who recorded the data and how.
Timing and spatial scale	Indicate the start and stop dates of data collection, noting the frequency and periodicity of sampling and providing a rationale for these choices. If there is a gap between collection periods, state the dates for each sample cohort. Specify the spatial scale from which the data are taken
Data exclusions	If no data were excluded from the analyses, state so OR if data were excluded, describe the exclusions and the rationale behind them, indicating whether exclusion criteria were pre-established.
Reproducibility	Describe the measures taken to verify the reproducibility of experimental findings. For each experiment, note whether any attempts to repeat the experiment failed OR state that all attempts to repeat the experiment were successful.
Randomization	Describe how samples/organisms/participants were allocated into groups. If allocation was not random, describe how covariates were controlled. If this is not relevant to your study, explain why.
Blinding	Describe the extent of blinding used during data acquisition and analysis. If blinding was not possible, describe why OR explain why blinding was not relevant to your study.

Did the study involve field work?  Yes  No

## Field work, collection and transport

Field conditions	Describe the study conditions for field work, providing relevant parameters (e.g. temperature, rainfall).
Location	State the location of the sampling or experiment, providing relevant parameters (e.g. latitude and longitude, elevation, water depth).
Access and import/export	Describe the efforts you have made to access habitats and to collect and import/export your samples in a responsible manner and in compliance with local, national and international laws, noting any permits that were obtained (give the name of the issuing authority, the date of issue, and any identifying information).
Disturbance	Describe any disturbance caused by the study and how it was minimized.

## Reporting for specific materials, systems and methods

**Materials & experimental systems**

n/a	Involved in the study
<input checked="" type="checkbox"/>	<input type="checkbox"/> Unique biological materials
<input type="checkbox"/>	<input checked="" type="checkbox"/> Antibodies
<input type="checkbox"/>	<input checked="" type="checkbox"/> Eukaryotic cell lines
<input checked="" type="checkbox"/>	<input type="checkbox"/> Palaeontology
<input checked="" type="checkbox"/>	<input type="checkbox"/> Animals and other organisms
<input type="checkbox"/>	<input checked="" type="checkbox"/> Human research participants

**Methods**

n/a	Involved in the study
<input checked="" type="checkbox"/>	<input type="checkbox"/> ChIP-seq
<input type="checkbox"/>	<input checked="" type="checkbox"/> Flow cytometry
<input checked="" type="checkbox"/>	<input type="checkbox"/> MRI-based neuroimaging

## Unique biological materials

Policy information about [availability of materials](#)

## Obtaining unique materials

*Describe any restrictions on the availability of unique materials OR confirm that all unique materials used are readily available from the authors or from standard commercial sources (and specify these sources).*

## Antibodies

## Antibodies used

Anti-IFNAR antibody, cat. number 21385-1, PBL Inferon Source, Piscataway, USA

## Validation

The antibody was validated by the manufacturer. Neutralization effect of anti-IFNAR antibody on human interferon-alpha 2a and interferon beta was done on A549 cells using cytopathic effect inhibition assay. Relevant data is available at the manufacturer's website.

## Eukaryotic cell lines

Policy information about [cell lines](#)

## Cell line source(s)

Vaginal epithelial cells A431, obtained from DSMZ, described in Methods section, paragraph "In vitro vaginal epithelial infection model"  
Primary human vaginal ECs (ATCC® PCS-480-010™), obtained from ATCC, described in Methods section, paragraph "Primary vaginal cells"

## Authentication

A431 cells were authenticated regularly by STR analysis, Primary vaginal cells were not authenticated.

## Mycoplasma contamination

Mycoplasma contamination was routinely checked and the results were negative.

Commonly misidentified lines  
(See [ICLAC](#) register)

No misidentified cell lines used

## Palaeontology

## Specimen provenance

*Provide provenance information for specimens and describe permits that were obtained for the work (including the name of the issuing authority, the date of issue, and any identifying information).*

## Specimen deposition

*Indicate where the specimens have been deposited to permit free access by other researchers.*

## Dating methods

*If new dates are provided, describe how they were obtained (e.g. collection, storage, sample pretreatment and measurement), where they were obtained (i.e. lab name), the calibration program and the protocol for quality assurance OR state that no new dates are provided.*

Tick this box to confirm that the raw and calibrated dates are available in the paper or in Supplementary Information.

## Animals and other organisms

Policy information about [studies involving animals](#); [ARRIVE guidelines](#) recommended for reporting animal research

## Laboratory animals

*For laboratory animals, report species, strain, sex and age OR state that the study did not involve laboratory animals.*

## Wild animals

*Provide details on animals observed in or captured in the field; report species, sex and age where possible. Describe how animals were caught and transported and what happened to captive animals after the study (if killed, explain why and describe method; if released, say where and when) OR state that the study did not involve wild animals.*

## Field-collected samples

*For laboratory work with field-collected samples, describe all relevant parameters such as housing, maintenance, temperature, photoperiod and end-of-experiment protocol OR state that the study did not involve samples collected from the field.*

## Human research participants

Policy information about [studies involving human research participants](#)

Population characteristics	No covariate-relevant population characteristics have been obtained.
Recruitment	Blood donors were healthy volunteers, who provided written informed consent (Methods section, paragraph "Blood donors"). Healthy volunteers in our study are employees of Leibniz-HKI (Jena). There are no relevant biases that may impact results, as this group consists of both female and male participants, in good general health condition and the wide age range.

## ChIP-seq

### Data deposition

- Confirm that both raw and final processed data have been deposited in a public database such as [GEO](#).
- Confirm that you have deposited or provided access to graph files (e.g. BED files) for the called peaks.

#### Data access links

*May remain private before publication.*

For "Initial submission" or "Revised version" documents, provide reviewer access links. For your "Final submission" document, provide a link to the deposited data.

#### Files in database submission

Provide a list of all files available in the database submission.

#### Genome browser session (e.g. [UCSC](#))

Provide a link to an anonymized genome browser session for "Initial submission" and "Revised version" documents only, to enable peer review. Write "no longer applicable" for "Final submission" documents.

### Methodology

#### Replicates

Describe the experimental replicates, specifying number, type and replicate agreement.

#### Sequencing depth

Describe the sequencing depth for each experiment, providing the total number of reads, uniquely mapped reads, length of reads and whether they were paired- or single-end.

#### Antibodies

Describe the antibodies used for the ChIP-seq experiments; as applicable, provide supplier name, catalog number, clone name, and lot number.

#### Peak calling parameters

Specify the command line program and parameters used for read mapping and peak calling, including the ChIP, control and index files used.

#### Data quality

Describe the methods used to ensure data quality in full detail, including how many peaks are at FDR 5% and above 5-fold enrichment.

#### Software

Describe the software used to collect and analyze the ChIP-seq data. For custom code that has been deposited into a community repository, provide accession details.

## Flow Cytometry

### Plots

Confirm that:

- The axis labels state the marker and fluorochrome used (e.g. CD4-FITC).
- The axis scales are clearly visible. Include numbers along axes only for bottom left plot of group (a 'group' is an analysis of identical markers).
- All plots are contour plots with outliers or pseudocolor plots.
- A numerical value for number of cells or percentage (with statistics) is provided.

### Methodology

#### Sample preparation

Epithelial cells were stained with 20nM MitoTracker® Deep Red FM for 15 min at 37°C, detached using Accutase®, and fixed with Roti®-Histofix 4%. After three washing steps with PBS, epithelial cells were resuspended in 1 ml PBS and analysed by Flow Cytometry. Non-stained uninfected epithelial cells were included as control.

#### Instrument

BD FACS Verse®. BD Biosciences, Franklin Lakes, USA

#### Software

BD FACSuite v1.0.6.5230 was used to collect data. Data was analysed using the software FlowJo v10.2.

#### Cell population abundance

No cell sorting was performed.

## Gating strategy

The gating strategy is shown in Extended Data Fig. 8 for both epithelial cell lines used in this study.

Tick this box to confirm that a figure exemplifying the gating strategy is provided in the Supplementary Information.

## Magnetic resonance imaging

### Experimental design

## Design type

Indicate task or resting state; event-related or block design.

## Design specifications

Specify the number of blocks, trials or experimental units per session and/or subject, and specify the length of each trial or block (if trials are blocked) and interval between trials.

## Behavioral performance measures

State number and/or type of variables recorded (e.g. correct button press, response time) and what statistics were used to establish that the subjects were performing the task as expected (e.g. mean, range, and/or standard deviation across subjects).

### Acquisition

## Imaging type(s)

Specify: functional, structural, diffusion, perfusion.

## Field strength

Specify in Tesla

## Sequence &amp; imaging parameters

Specify the pulse sequence type (gradient echo, spin echo, etc.), imaging type (EPI, spiral, etc.), field of view, matrix size, slice thickness, orientation and TE/TR/flip angle.

## Area of acquisition

State whether a whole brain scan was used OR define the area of acquisition, describing how the region was determined.

## Diffusion MRI

Used

Not used

### Preprocessing

## Preprocessing software

Provide detail on software version and revision number and on specific parameters (model/functions, brain extraction, segmentation, smoothing kernel size, etc.).

## Normalization

If data were normalized/standardized, describe the approach(es): specify linear or non-linear and define image types used for transformation OR indicate that data were not normalized and explain rationale for lack of normalization.

## Normalization template

Describe the template used for normalization/transformation, specifying subject space or group standardized space (e.g. original Talairach, MNI305, ICBM152) OR indicate that the data were not normalized.

## Noise and artifact removal

Describe your procedure(s) for artifact and structured noise removal, specifying motion parameters, tissue signals and physiological signals (heart rate, respiration).

## Volume censoring

Define your software and/or method and criteria for volume censoring, and state the extent of such censoring.

### Statistical modeling & inference

## Model type and settings

Specify type (mass univariate, multivariate, RSA, predictive, etc.) and describe essential details of the model at the first and second levels (e.g. fixed, random or mixed effects; drift or auto-correlation).

## Effect(s) tested

Define precise effect in terms of the task or stimulus conditions instead of psychological concepts and indicate whether ANOVA or factorial designs were used.

## Specify type of analysis:

Whole brain     ROI-based     Both

Statistic type for inference  
(See [Eklund et al. 2016](#))

Specify voxel-wise or cluster-wise and report all relevant parameters for cluster-wise methods.

## Correction

Describe the type of correction and how it is obtained for multiple comparisons (e.g. FWE, FDR, permutation or Monte Carlo).

### Models & analysis

## n/a

## Involved in the study

- Functional and/or effective connectivity
- Graph analysis
- Multivariate modeling or predictive analysis

## Functional and/or effective connectivity

Report the measures of dependence used and the model details (e.g. Pearson correlation, partial correlation, mutual information).

## Graph analysis

Report the dependent variable and connectivity measure, specifying weighted graph or binarized graph,

Graph analysis

*subject- or group-level, and the global and/or node summaries used (e.g. clustering coefficient, efficiency, etc.).*

Multivariate modeling and predictive analysis

*Specify independent variables, features extraction and dimension reduction, model, training and evaluation metrics.*